Structural Preference for Changes in the Direction of the Ca^{2+}-Induced Transition: A Study of the Regulatory Domain of Skeletal Troponin-C

Felicia Pitici
Department of Chemistry, Wesleyan University, Middletown, Connecticut 06459 USA

ABSTRACT The determinants for specificity in the Ca^{2+}-dependent response of the regulatory N-terminal domain of skeletal troponin-C are a combination of intrinsic and induced properties. We characterized computationally the intrinsic propensity of this domain for structural changes similar to those observed experimentally in the Ca^{2+}-induced transition. The preference for such changes was assessed by comparing the structural effect of the harmonic and quasiharmonic vibrations specific for each Ca^{2+} occupancy with crystallographic data. Results show that only the Ca^{2+}-saturated form of the protein features a slow vibrational motion preparatory for the transition. From the characteristics of this mode, we identified a molecular mechanism for transition, by which residues 42-51 of helix B and of the adjacent linker move toward helices (A, D), and bind to the surface used by the protein to interact with troponin-I. By obstructing the access of the target to hydrophobic residues important in the formation of the complex, helix B and the adjacent linker act as an autoinhibitory structural element. Specific properties of the methionines at the interaction surface were found to favor the binding of the autoinhibitory region. Located over hydrophobic residues critical for binding, the methionines are easily displaceable to increase the accessibility of these residues to molecular encounter.

INTRODUCTION

Troponin-C (TnC) is the Ca^{2+}-sensing component of a protein complex that regulates the contraction-relaxation cycle in skeletal and cardiac muscle. TnC acts in conjunction with two other molecules, troponin-I (TnI) and troponin-T (TnT), which attach the complex to the muscle fiber through interactions with actin and tropomyosin (Ruegg, 1986). Upon surges in the cellular concentration of Ca^{2+} to $\sim 10\mu$M, TnC chelates ions to low-affinity binding sites and becomes functionally active, capable of transmitting the Ca^{2+} signal to TnI and further, to the motor molecules actin and myosin, (Cohen, 1975; Leavis and Gergely, 1984). The ability of TnC to transduce the Ca^{2+} signal has been ascribed to its large structural response to binding four Ca^{2+}, which leads to a conformation favoring the formation of Ca^{2+}-dependent interactions with TnI (Grabareck et al., 1981). The structural changes initiated in the regulatory complex propagate throughout the muscle fiber to actin and myosin, whose relative movement generates the contraction force (Ruegg, 1986).

Structural data for the skeletal isoform of TnC (sTnC) and for sTnC-derived tryptic fragments provide an accurate description of the conformational changes associated with Ca^{2+}-binding (Herzberg and James, 1988; Slupsky and Sykes, 1995; Houdusse et al., 1997; Gagne et al., 1995; Strynadka et al., 1997). The elements of structure involved in the recognition of the Ca^{2+}-signal are two pairs of helix-loop-helix motifs of the EF-hand type (Kretsinger, 1980), each located in spatially separated globular domains. Ca^{2+}-sensing properties are specific for individual domains, of which the N-terminal one (N-sTnC) includes the low-affinity binding sites, regulatory for function (Zot and Potter, 1982). The domain organization in the absence and presence of Ca^{2+} is illustrated in Fig. 1 for N-sTnC, the fragment chosen as model system in our computational studies. This option was prompted by findings from NMR spectroscopy that N-sTnC retains the structural and Ca^{2+}-binding properties of the analogous region from the full-length protein (Li et al., 1995). The availability of structural and mechanistic data for the Ca^{2+}-induced transition was also considered important because it yields the comparison set of properties needed to validate the calculations. An additional advantage of this choice is purely technical, in that it provides an almost globular molecular frame, amenable to accurate representations by computational protocols.

The conformations attained by N-sTnC in the transition have been characterized as closed and open, to reflect the relative position of the component helices (Gagne et al., 1995). The closed conformation corresponds to the functionally inactive apo state, and features a compact arrangement of the helices via numerous mutual contacts. Upon saturation with Ca^{2+}, the domain undergoes large structural changes that favor the exposure of hydrophobic residues used to interact with the TnI target (McKay et al., 1997, 1998). The energetic cost for bringing these residues at the protein surface is compensated by the enthalpy of binding Ca^{2+} at the two EF-hand loops. The Ca^{2+}-induced structural response has been characterized as an opening, because it

Submitted March 15, 2002, and accepted for publication September 5, 2002.

Address reprint requests to Felicia Pitici, E-mail: fpitici@wesleyan.edu.

Abbreviations used: TnC, troponin-C; sTnC, skeletal TnC; N-sTnC, the N-terminal domain of sTnC; CaM, calmodulin; TnI, troponin-I; TnT, troponin-T; MLCK, myosin light chain kinase; MD, molecular dynamics; FCC, face-centered-cubic; SD, steepest descent; ABNR, adopted basis Newton Raphson; NM, normal mode; H, harmonic; QH, quasiharmonic; mode-1H and mode-1QH, the first harmonic and quasiharmonic vibrational mode, respectively; rms, root-mean-square; LCC, linear correlation coefficient.

0006-3495/03/01/82/20 $2.00

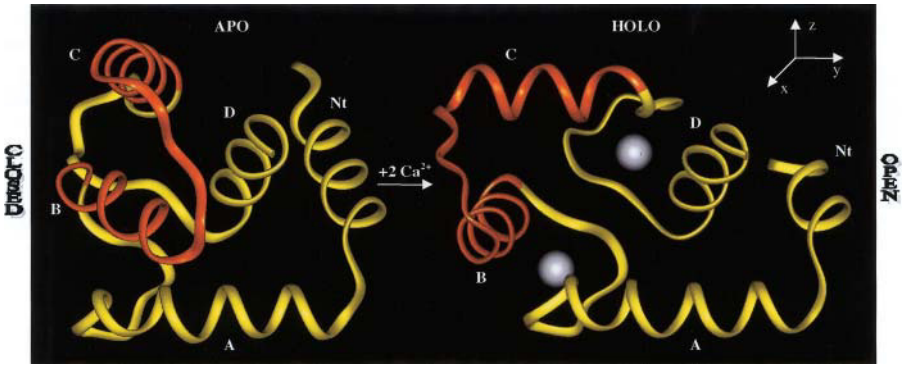

FIGURE 1 Ca^{2+}-induced conformational change of N-sTnC: relative displacement of helices (B, C) and of the adjoining linker away from the group of helices (Nt, A, D) (*structural groups were colored orange and yellow, respectively*). The Ca^{2+}-free (*apo*) and the Ca^{2+}-bound (*holo*) molecules were oriented by a least-squares fit of the C_α-atoms of helices Nt, A, and D (rms = 0.9 Å). Labels indicate the five α-helices and the casual characterization of the apo and holo conformations as closed and open, respectively. Helices of minimal length were defined to comprise residues that are in an α-helical conformation in both the apo and the holo states: Nt (5: 13), A (16: 30), B (38: 49), C (55: 65), and D (74: 84) (Gagne et al., 1995; Li et al., 1997). The x axis of the Cartesian reference system chosen in this study is orthogonal to the plane of the figure. Atomic coordinates were from the crystal structures of apo and holo sTnC (Herzberg and James, 1988; Houdusse et al., 1997).

involves large relative displacements of two structural blocks away from each other. The blocks comprise almost equal parts of the structure, formed of the middle pair of helices (B, C), and of the group of terminal helices (Nt, A, D).

The transition has been described from NMR determinations for the wild-type system and for a transition state analog, the E41A mutant (Li et al., 1995, 1997; Gagne et al., 1997). The mutant has been designed to probe the role of Glu-41, the residue at position 12 of the first Ca^{2+}-binding loop, in coupling Ca^{2+} binding to the conformational transition. The process involves sequential binding of Ca^{2+} to sites II and I with affinities of 1.7 μM and 16 μM, respectively. Structurally preformed for ligating Ca^{2+} with octahedral coordination symmetry, site II is not instrumental in triggering global conformational changes. The regulatory action of N-sTnC is manifested in the second step of the transition, when side-chain rearrangements at site I promote the opening of the structure. It has been assumed that Glu-41 triggers these changes, by acting as a hinge for rigid body displacements of the adjoining group of helices (B, C). The transition involves a singly Ca^{2+}-occupied intermediate which retains a closed conformation similar to that observed in the apo state, and which is therefore, functionally inactive.

Although the experiment yields high resolution structures for states of different Ca^{2+}-occupancy, and gives insight into the transition process, the molecular mechanisms involved are not yet fully understood. The comparison between the closed and open conformations yields an assessment of the structural changes induced by Ca^{2+}, with specifications for the internal coordinates determinant of molecular geometry. However, this set of parameters is not sufficient to characterize in absolute terms the atomic displacements leading to the observed changes, and thus cannot be used to outline the mechanistic aspects of the transition at molecular level. For example, an increased separation between two atoms is a relative measure that may result from various combinations of magnitude and directionality for the atomic displacements. In the simple one-dimensional case, an increase D could account, as well, for movements of the atoms in the same or in opposite directions with excursions of $(D + \delta, \delta)$ and $(D - \delta, \delta)$, respectively. Furthermore, the role of Glu-41 in the conformational transition is also not yet described in terms of the interactions and movements involved.

To identify properties determinant for the Ca^{2+}-dependent structural response of N-sTnC, we performed computational studies that employ methods of vibrational analysis and molecular dynamics (MD) simulations. Complementary to the experiment, these studies provide a theoretical framework for understanding the molecular mechanisms involved in the transition between closed and open conformations. The specific hypothesis investigated in our work is that the observed structural changes are determined as well by intrinsic factors preparatory for the transition. Such factors were sought for as low-frequency vibrations that produce displacements of the groups of helices (A, D) and (B, C) toward conformations characteristic of the closed or open form. These motions are of interest due to their high amplitude and delocalized effect, which determine large contributions to the structural fluctuations affecting the global fold of the protein. Existent as slow components of the protein dynamics, such vibrations yield a propensity for distorsions incipient of the structural changes specific for transition. The transition is nevertheless driven by Ca^{2+}, the external factor that could exploit this intrinsic preference to enhance the changes to amplitudes relevant for the process.

Notably, the idea that low-frequency vibrations prepare a molecule for function has led to interesting relationships for molecules as diverse as lysozyme (Brooks and Karplus, 1985), actin (Tirion and ben-Avraham, 1993), thermolysin

(Hayward et al., 1997), HIV-1 protease (Bahar et al., 1998), etc. The application to N-sTnC was thought as a prototype study of the transition mechanism for modulatory EF-hand Ca^{2+}-binding proteins, in direct surveillance of the experimental data. More general, this approach is suited for identifying properties determinant for functional differences among proteins of the EF-hand type.

An important, yet technical aspect of our work was to assess its predictive value by using the following criteria for validation: Results from vibrational analysis are model independent, and MD simulations yield relevant ensembles of states. The first objective was met by calculating the vibrational modes using two formulations, which have different model assumptions and address differently the convergence problem. In the normal mode (NM) analysis, for example, the atomic motions are treated as harmonic oscillations, and the modes from single point calculations sample the full conformational space (Clarage et al., 1995). In contrast, the quasiharmonic (QH) analysis incorporates anharmonic effects, but faces convergence problems due to restricted sampling of the atomic fluctuations in MD simulations (Balsera et al., 1996). Our reconcilable approach on the subject was to identify common structural and dynamic properties of the modes derived from NM and QH analyses.

The quality of the MD simulations used for QH analysis was assessed by comparing the calculated atomic fluctuations and the backbone ^{15}N order parameters with experimental data. Energetic and structural properties were also monitored for stability during the production runs. We consider that, by most criteria, the simulated systems have average physical properties close to those observed experimentally. Therefore, the ensembles selected for QH vibrational analysis include highly populated states, representative for systems in an aqueous environment.

The results from NM and QH analyses showed that the preference for changes in the direction of the transition is specific only for the Ca^{2+}-bound form of N-sTnC. Modes-1H and -2QH were found to initiate deformations of the holo structure to a more closed form that features a compact arrangement of the helices. Preparatory for the large structural changes characteristic for this step of the transition, the vibrations describe a movement of residues 42-51 toward the surface used to interact with the TnI target. Upon binding to the same surface, the mobile segment obstructs the access of the target to hydrophobic groups critical for the formation of the complex. We propose that residues 42-51, comprising helix B and adjacent linker residues, play an autoinhibitory structural role. The structural homology between this region and the target peptide from TnI further indicate that the autoinhibition is achieved by target mimetics.

In this representation, the holo→apo transition is an association process that involves binding of the autoinhibitory region to the interaction surface. Target encounter occurs in a competitive manner because it requires the same hydrophobic residues for interaction. The possible implications of our findings for understanding the Ca^{2+}-sensing action of N-sTnC are discussed in the closing section of the paper.

To assess the role of side-chain interactions in the adaptation for transition, we characterized the structural properties at the surface used to bind the autoinhibitory region and the TnI target. Met residues were found to adopt a specific arrangement at the binding surface of holo N-sTnC, by which their side chains occlude other hydrophobic residues. Due to high intrinsic flexibility and to weak interaction constraints, methionines are easily removable to uncover these residues to molecular encounter. Interestingly, we note the occurrence of Met-Phe pairs at the interaction surface, as an energetically favorable way to solvate the aromatic rings, while still placing minimal restraints on their accessibility for binding.

The results from computations yielded various contributions to the process of structural adaptation that marks the Ca^{2+}-sensing function of N-sTnC. Global changes from the open to the closed conformation were initiated by slow vibrations in the direction of the transition. From the concerted motions involved, we could identify residues and groups of residues likely to have mechanistic roles in the transition. Local side-chain properties were also found to favor the interactions with helix B and adjacent linker residues, which are required for the formation of the closed structure.

METHODS

Formulation of vibrational analysis

The underlying assumption of the formalism for vibrational analysis is that the protein is a generalized oscillator whose motion is described by the equation

$$\hat{\mathbf{M}}\ddot{\boldsymbol{\rho}} + \mathbf{K}\hat{\boldsymbol{\rho}} = 0, \tag{1}$$

where $\rho(t)$ is the displacement of the N-atomic system from equilibrium, $\hat{\boldsymbol{M}}$ is the mass matrix, and $\hat{\boldsymbol{K}}$ is the force constant matrix (Brooks et al., 1988). The solution of this equation is a superposition of 3N-6 independent vibrations, $\{\rho^{\alpha}(t)\}$,

$$\rho(\mathrm{t}) = \sum_{\alpha=7}^{3\mathrm{N}} \rho^{\alpha}(\mathrm{t}), \tag{2}$$

each mode α being characterized by three parameters: direction a^{α}, frequency ω_{α}, and phase φ_{α}. One component of the displacement vector $\rho(t)$ is, for example, the displacement of atom n from the equilibrium position

$$\vec{\boldsymbol{\rho}}_{\mathrm{n}}(\mathrm{t}) = \left(\frac{\mathrm{k_b T}}{\mathrm{m_n}}\right)^{1/2} \sum_{\alpha=7}^{3\mathrm{N}} \frac{\vec{\mathbf{a}}_{\mathbf{n}}^{\boldsymbol{\alpha}}}{\boldsymbol{\omega}_{\alpha}} \cos(\omega_{\alpha}\mathrm{t} + \varphi_{\alpha}), \tag{3}$$

where $\vec{a}_n^{\alpha}$ is the component of a^{α} that corresponds to atom n, m_n is the mass of atom n, k_b is the Boltzmann constant, and T is the absolute temperature.

The force constant matrix, $\hat{\boldsymbol{K}}$, was determined using two different methods: the NM analysis, in which matrix elements are the second order derivatives of the potential function with respect to the atomic coordinates, estimated at a local minimum state

$$K^{xx}_{nn'} = \frac{1}{2}\left(\frac{\partial^2 V}{\partial x_n \partial x_{n'}}\right)_0, \tag{4}$$

and the QH analysis, in which they are related to the atomic displacements sampled with MD simulations

$$\begin{aligned} K^{xx}_{nn'} &= k_b T (\hat{Cov}^{-1})^{xx}_{nn'} \\ (\hat{Cov})^{xx}_{nn'} &= \langle (x_n - \langle x_n \rangle)(x_{n'} - \langle x_{n'} \rangle) \rangle. \end{aligned} \tag{5}$$

In the above relations, V is the potential function, $\hat{Cov}$ is the covariance matrix, $x_n - \langle x_n \rangle$ is the displacement of atom n from equilibrium along the x-direction, and the brackets represent time-averaging over states sampled in the simulation. Similar matrix elements were defined for other combinations of Cartesian coordinates: xy, xz, yy, yz, and zz.

System preparation

The atomic coordinates for apo N-sTnC were taken from the crystal structure of the intact protein (Herzberg and James, 1988). The availability of coordinates for holo N-sTnC at the onset of the computations determined different choices for the initial structure used in NM and QH analysis. For NM analysis, the coordinates were obtained from the crystal structure of the domain (Strynadka et al., 1997), whereas for the QH analysis they were taken from the solution structure of the intact protein (Gagne et al., 1995). The domain structures derived from intact proteins were obtained upon breaking the peptide bond at the tryptic cleavage site Lys-87 and adding a carbonyl group at the C terminus. The N-terminal residue of apo sTnC and the first six residues of holo N-sTnC, which were not defined in the crystal structure, were built in an extended conformation. The holo conformation chosen from the ensemble of NMR structures had the lowest root-mean-square (rms) deviation from the average structure.

Computations were carried out using the CHARMM force field (Brooks et al., 1983) with the all-hydrogen atom representation (MacKerell et al., 1998). Different system preparations were required for the calculation of the vibrational modes in the harmonic and QH approximation.

For NM analysis, each system was minimized with the conjugate gradient method to an equilibrium state close to that corresponding to the x-ray structure (Herzberg and James, 1988; Strynadka et al., 1997). The minimization to an energy gradient of 10^{-4} kcal/mole/Å produced structures within 1.5 Å rms deviation of the C_α-atoms from the starting conformation. Atomic interactions were estimated using an infinite cutoff and a linear distance-dependent dielectric function (Janezic and Brooks, 1995a; Janezic et al., 1995b).

For the QH analysis, the molecular motion of each of the apo and holo proteins was simulated for 1 ns using MD protocols. Solvation effects were modeled by a discrete representation of TIP3 water molecules (Jorgensen et al., 1983) in a cell with face-centered-cubic (FCC) symmetry. Nonbonded interactions were truncated at 13 Å using the shift and switch functions for the electrostatic and van der Waals components, respectively. Electrostatic interactions were estimated using a unit dielectric constant.

To ensure optimal solvation in the symmetry cell, the molecules were first immersed in large water spheres, of radius 44 Å, centered in the corresponding center of mass (Biosym Technologies, 1998). Each system was minimized using a protocol that combined the steepest descent (SD) and the adopted basis Newton Raphson (ABNR) methods. The solvent sphere was energy minimized for 500 steps of SD, and 1000 steps of ABNR, during which protein atoms were fixed. Additional minimization was performed for the built residues and the water molecules, and then for the total system (1000 steps of ABNR for each procedure). After the optimization of this initial model, the FCC cell was trimmed with Simulaid (Mezei, 1997) to ensure a minimal distance of 26 Å between protein images. The symmetry cells for apo and holo N-sTnC have edges of 42.6 Å and 44.9 Å, and comprise 5150 and 5677 water molecules, respectively. After the truncation of the symmetry cell, water molecules were minimized for 1000 steps of ABNR, and equilibrated for 140 ps of MD simulation in the mean field of the restrained protein. The starting structure for the all-atom simulation was the last snapshot from water equilibration, minimized for 1000 more steps of ABNR. Production runs of 1 ns were further conducted for the unrestrained system.

The MD simulations were carried out using the following protocol: heating to 300 K in increments of 5 K every 100 steps, and equilibration at 300 K with thermal fluctuations below 5 K. The integration step was 1.5 fs in simulations of the solvent, and 1 fs for the entire system. The list of nonbonded interacting atoms and the image list were updated every five steps. High-frequency motions involving hydrogen atoms were constrained with SHAKE (Ryckaert et al., 1977).

Computation and selection of vibrational modes

After the minimization and the MD protocol described above, the vibrational modes were computed using the CHARMM force field (Brooks et al., 1983) with the all-hydrogen atom representation (MacKerell et al., 1998). Two subroutines of the chemistry software were employed to compute the harmonic and QH modes (Brooks et al., 1995). Rigid-body motions were removed before the calculation of the QH modes by orienting each trajectory to a reference structure, chosen to be the corresponding minimized structure from NM analysis.

The minimal basis set of vibrational modes that still describes adequately the protein motion was defined for each system according to the contribution of the modes to the total fluctuations. For example, the structural fluctuations produced by mode α are

$$F(\alpha) = \langle (\rho^\alpha(t) - \langle \rho^\alpha(t) \rangle)^2 \rangle, \tag{6}$$

where the brackets represent time averaging over the period of the vibrational motion. Because the components of the 3N-dimensional vector $\rho^\alpha(t)$ are given by the generic term in expression 3, $F(\alpha)$ can be written in terms of the atomic masses and mode parameters

$$F(\alpha) = \frac{k_b T}{2} \sum_{n=1}^{N} \frac{1}{m_n} \left(\frac{\vec{a}^{\alpha}_n}{\omega_\alpha}\right)^2. \tag{7}$$

Using these notations for individual modes, the contribution (%) of the first M low-frequency vibrations to the total atomic fluctuations is given by

$$P(M) = \frac{\sum_{\alpha=7}^{M+6} F(\alpha)}{\sum_{\alpha=7}^{3N} F(\alpha)} 100 = \frac{\sum_{\alpha=7}^{M+6} \sum_{n=1}^{N} \frac{1}{m_n} \left(\frac{\vec{a}^{\alpha}_n}{\omega_\alpha}\right)^2}{\sum_{\alpha=7}^{3N} \sum_{n=1}^{N} \frac{1}{m_n} \left(\frac{\vec{a}^{\alpha}_n}{\omega_\alpha}\right)^2} 100. \tag{8}$$

Description of structural differences

Conformational states of the protein were compared using a structural descriptor defined from the elements of the difference distance matrix (Liebman at al., 1985) that corresponds to the selected pair of states. In this representation, a conformational state is described by a distance matrix of elements equal to the interatomic distances $\{d_{nm}\}$ for all pairs of atoms (n,m). The structural differences between two states are given by the difference distance matrix $\{d'_{nm} - d_{nm}\}$ calculated from the individual distance matrices. The descriptor used for structural analysis was defined as a vectorial array of components equal to the elements of the difference distance matrix

$$\begin{aligned} D = (&d'_{12} - d_{12}, \ldots, d'_{1N'} - d_{1N'}, d'_{23} - d_{23}, \ldots, \\ &d'_{N'-1N'} - d_{N'-1N'}), \end{aligned} \tag{9}$$

where N' is the number of selected protein atoms. The analysis was

performed for $N' = 86$, the number of protein residues, and the generalized vector D was calculated from the coordinates of the C_α-atoms.

Computation of other properties

Structural fluctuations

Under the assumption that the atomic motions are isotropic and harmonic, the mean-square fluctuations, $\langle(\Delta r_n)^2\rangle$, are proportional to the crystallographic temperature factors, B_n (Willis and Pryor, 1975)

$$\langle(\Delta r_n)^2\rangle = \frac{3B_n}{8\pi^2}. \quad (10)$$

This relationship was used to compare the fluctuations computed from MD simulations with the measured *B*-factors . To characterize only intrinsic vibrations, as determined experimentally, the atomic fluctuations were calculated from a trajectory modified to project out overall domain motions. Rigid-body motions were removed using a least-squares fit (Kabsch, 1976) of each entry in the trajectory relative to the starting structure.

Order parameters

The generalized order parameter, S^2, measures the extent of reorientation of the N-H bond vector due to internal backbone motion. Its value ranges from 0, for free, isotropic motion, to 1 for totally restricted motion.

In the model free formalism proposed by Lipari and Szabo (Lipari and Szabo, 1982), the order parameter is related to the autocorrelation function, $C_\alpha(t)$, that describes the relaxation of bond rotation

$$C_\alpha(t) = \langle P_2(\vec{v}_\alpha(\tau) \times \vec{v}_\alpha(t+\tau))\rangle, \quad (11)$$

where P_2 is the second-order Legendre polynomial, $\vec{v}_\alpha(t)$, is the instantaneous N-H unit vector in a protein fixed-frame reference system, and the angle brackets denote time averaging. The order parameter of each N-H bond is the asymptotic limit of the corresponding autocorrelation function

$$S^2 = \lim_{t\to\infty} C(t) = \frac{4\pi}{3}\sum_{m=-2}^{2} |Y_{2m}(\Omega)|^2, \quad (12)$$

where Y_{2m} are the second-order spherical harmonics, and Ω is the orientation of the N-H bond vector relative to a molecular fixed frame.

Consistent with the formalism, the atomic coordinates from simulations were expressed in the protein fixed-frame reference system using the orientational procedure described above. Because this procedure corresponds to the model assumptions for the interpretation of NMR data (Gagne et al., 1998), the calculated order parameters could be compared with the experimental values.

RESULTS

Mode calculation

The procedure outlined in the Methods section was used to prepare the apo and holo proteins for vibrational analysis, and to calculate the harmonic and QH modes. For QH analysis, the calculation included states sampled with MD simulations that, by most criteria, describe average structural and dynamic properties close to those observed experimentally (see Appendix).

The vibrational modes were calculated using both the harmonic and the QH approximation because each formalism has a different underlying set of assumptions and addresses differently the convergence problem. Although atomic motions are described as harmonic oscillations in the NM analysis, the QH analysis includes some anharmonic effects as sampled with MD simulations. On the other hand, slow vibrational modes may be undersampled in the simulation, whereas there is no such limitation in the NM analysis (Clarage et al., 1995; Balsera et al., 1996). Despite the convergence issue raised by these authors, a series of computations have shown that 1 ns-long MD simulations can sample essential motions related to functional properties (van Aalten et al., 1995a, 1995b; Hayward et al., 1997). To reconcile these statements and to extract structural and dynamic properties that are model independent, we searched for commonalities of the modes from the two analyses.

Selection and sampling of dominant vibrations

The solution of the generalized eigenvalue problem from vibrational analysis yields a set of $3N - 6$ vibrational modes, where $N = 1312/1320$ for apo/holo N-sTnC. Because such a large basis set was not amenable for further analysis, the modes were selected according to their contribution to the total structural fluctuations of the protein. As described in the Methods section, the contribution, $P(M)$, of selected modes to the total fluctuations can be expressed in terms of the corresponding amplitudes and frequencies of the modes, weighted by the atomic masses (Eq. 8).

This selection criterion was applied to the vibrational modes from harmonic and QH analysis for each of the apo and holo proteins. Results show that the first 30 low-frequency modes from each calculation account for more than half of the total structural fluctuations (Fig. 2). The corresponding eigenvectors form minimal basis sets that still describe adequately the structural and dynamic properties of the proteins. These sets of vectors were considered representative for each system and were, therefore used for further analysis.

Due to the limited sampling of slow motions in MD simulations, it is important to characterize carefully the QH modes that correspond to low frequencies. A suitable approach was to decompose the motion of the protein into components along the directions $\{a^\alpha\}$ of these modes (Amadei et al., 1993). For this purpose, the dynamics data from simulations were viewed as series of 3N-dimensional vectors, $\{r(t)\}$, each vector including all atomic coordinates at a given instance. The component of motion along each vector a^α was described by the projections of vectors $\{r(t)\}$ onto a^α, as defined by the generalized dot product $r(t) \cdot a^\alpha$.

Results are shown only for the first four QH modes (Fig. 3), because at higher frequencies the projections have similar patterns reflecting the localized character of the motion. The time variation of the projections and the corresponding distribution functions indicate that the component of motion along the first QH eigenvector is affected by anharmonicity. Such effects are illustrated by the drift of the projected coordinates in the course of the simulation, and by the

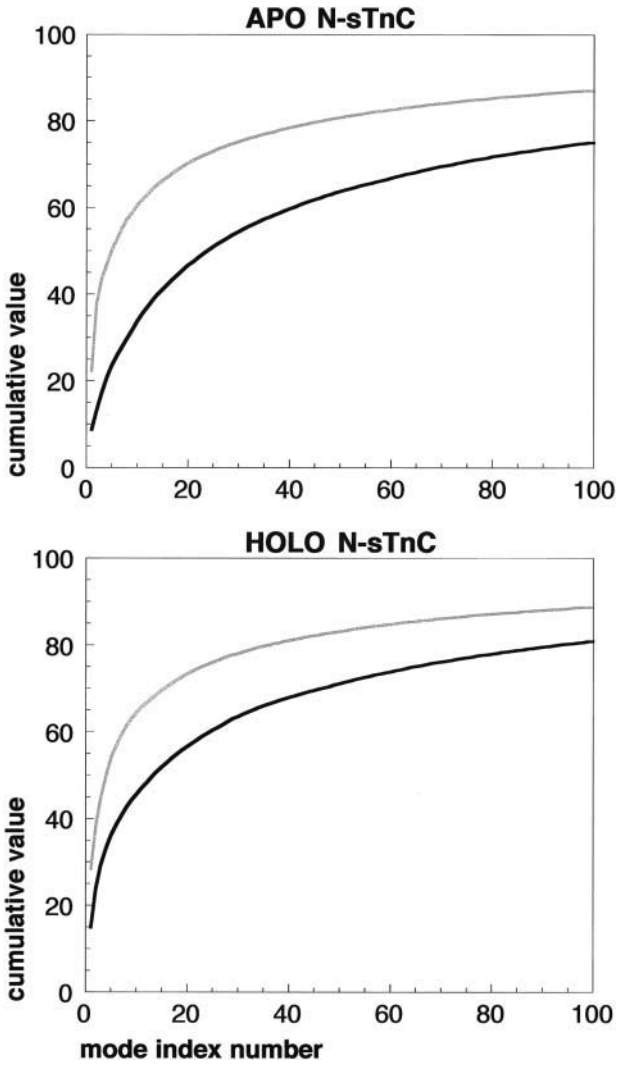

FIGURE 2 Cumulative contribution of the vibrational modes of apo and holo N-sTnC to the total structural fluctuations. Results shown for the first 100 low-frequency modes computed from NM (*gray*) and from QH (*black*) analysis.

multimodal character of the distributions. As expected, the largest amplitude motion occurs along the direction of this first mode, with a deflexion at k_bT of 4.9/6.8 nm for apo/holo N-sTnC. The effect of anharmonicity on the lowest-frequency mode would be reflected by the structural and dynamic properties characteristic of this motion. Therefore, if mode-1QH had to be used to analyze changes in structure, then the interpretation of the results would have had to characterize such anharmonic effects and the observed interference with the vibrational motion.

Functional role of intrinsic vibrations

Search for modes preparatory for the transition

To search for modes that produce structural changes similar to those observed in the Ca^{2+}-induced transition, we assessed the structural effect of each selected dominant mode and compared it with the experimental changes. The analysis was conducted using multidimensional vectors, D, defined in the Methods section as descriptors of the structural differences between two selected states. The components of D are difference distances, $\{d'_{nm} - d_{nm}\}$, calculated from the coordinates of the compared structures for all pairs of C_α-atoms (n, m) (Eq. 9).

The structural effect of each mode was described by the largest deviation of the system from equilibrium due to a vibrational motion of total energy k_bT. To characterize such changes, the reference structure was chosen at equilibrium and the most deformed structure at the amplitude of vibration. The coordinates of the structure attained at the amplitude of vibration were determined from the generic term in Eq. 3, using parameters characteristic for each mode. The components of each vector $D_{calc}(\alpha)$ were then calculated as difference distances between the two selected states that correspond to mode α.

The comparison term, D_{exp}, required for analysis was obtained from data that describe experimentally the Ca^{2+}-induced conformational change. Because both apo and holo N-sTnC have been determined at high resolution (Herzberg and James, 1988; Strynadka et al., 1997), we used the atomic coordinates to estimate the difference distances that define D_{exp}.

The relationship between the calculated and the experimental structural changes was characterized for each mode α by linear regression between the components of vectors $D_{calc}(\alpha)$ and D_{exp}. An illustration of the results from this comparison is given in Fig. 4 for the first two harmonic modes of the holo protein. Similar relationships were established for each of the first 30 low-frequency harmonic and QH modes that were selected for analysis. The degree of correlation between the calculated and the experimental data was assessed quantitatively using linear correlation coefficients (LCC) (Fig. 5). High correlations were found only for modes-1H and -2QH of the holo protein, for which LCC = 0.88 and 0.71, respectively. This indicates a high similarity between the structural effect of the two modes and the changes observed experimentally in the transition.

To better characterize the observed similarity for modes-1H and -2QH of the holo protein, the calculated and the experimental changes were decomposed into contributions from individual helices or groups of helices relevant for the transition. The corresponding generalized vectors D were, therefore considered as superposition of four vectors

$$D = D(B) + D(C) + D(B, C) + D(Nt, A, D), \qquad (13)$$

where D(B) and D(C) include displacements of helices B and C, respectively, from the group of helices (Nt, A, D), and the last two terms describe structural changes within the groups of helices (B, C) and (Nt, A, D). The contribution of each

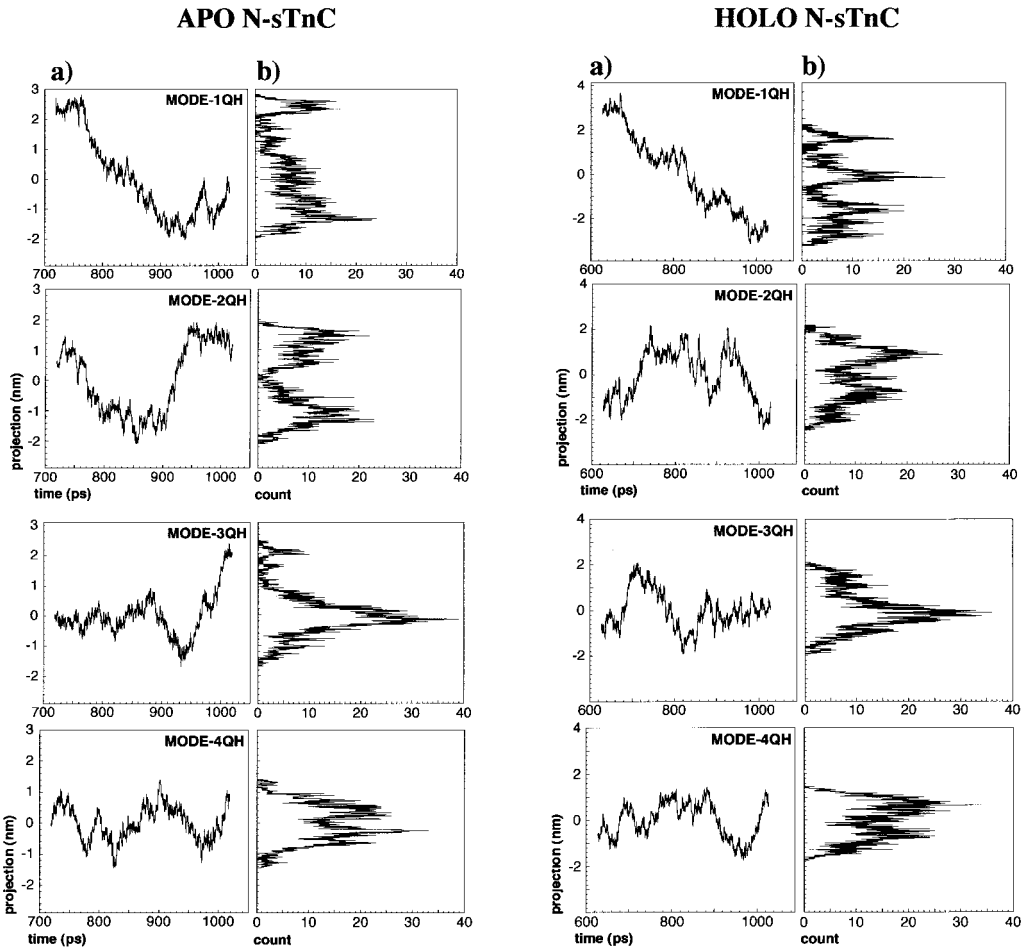

FIGURE 3 Components of the MD trajectories along the directions defined by the first four eigenvectors of apo and holo N-sTnC. Projection values (*a*) and the corresponding distributions (*b*) were calculated from the trajectory intervals considered for QH analysis (see Appendix).

term to the total correlation was assessed by the same procedure as described above for the resultant vector.

The components of the vectors calculated for each of modes-1H and -2QH of the holo protein were compared with the corresponding experimental values (Fig. 6). Correlations higher than the overall value were obtained for vectors D(B) and D(C): e.g., for mode-2QH, LCC = 0.85 and 0.84, respectively, versus the total coefficient of 0.71. This ascertains that modes-1H and -2QH describe the main characteristics of the conformational transition, which features large displacements of helices B and C relative to the (Nt, A, D) group. The lower total correlation of 0.71 reflects a slight negative coupling between the relative movement of helices B and C.

Results show that the preference of N-sTnC for structural changes in the direction of the transition is specific for each Ca^{2+} occupancy. The protein was found to undergo a slow vibrational motion preparatory for the transition only in the Ca^{2+}-bound state. This intrinsic motion produces distortions toward the apo conformation, thus enhancing the sensitivity of the holo protein to perturbations in Ca^{2+} ligation. In contrast to the holo state, protein dynamics does not support the conformational transition in the absence of Ca^{2+}. Without a preference for changes in the direction of the transition, the apo protein is expected to have a small structural response to Ca^{2+}.

Supported by two different formulations of vibrational analysis, our findings are consistent with the transition scheme proposed by Sykes et al. (Li et al., 1995). According to this scheme, the protein undergoes large structural rearrangements only in the first step of the holo→apo transition. The holo, but not the apo protein is, therefore prone to major conformational changes in this process.

Molecular mechanism for the holo→apo transition

To identify molecular mechanisms involved in the holo→apo transition, we further characterized modes-1H and -2QH, that were found to distort the holo protein toward the apo conformation. The underlying assumption for this

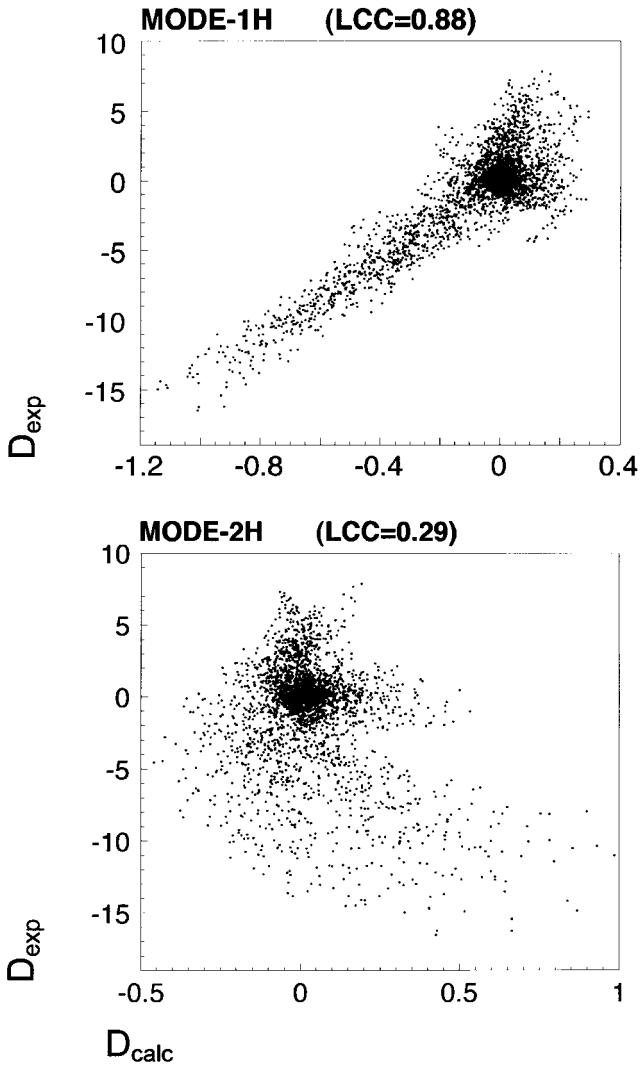

FIGURE 4 Correlation between the deformations produced by modes-1H and -2H of holo N-sTnC and the structural changes observed experimentally in the holo→apo transition. The components of vectors D_{calc} and D_{exp} were calculated as difference distances between sets of structures from calculation and experiment, respectively. Difference distances for each pair of C_α-atoms (n, m) are expressed in Å. Linear correlation coefficients (LCC) are indicated for each mode.

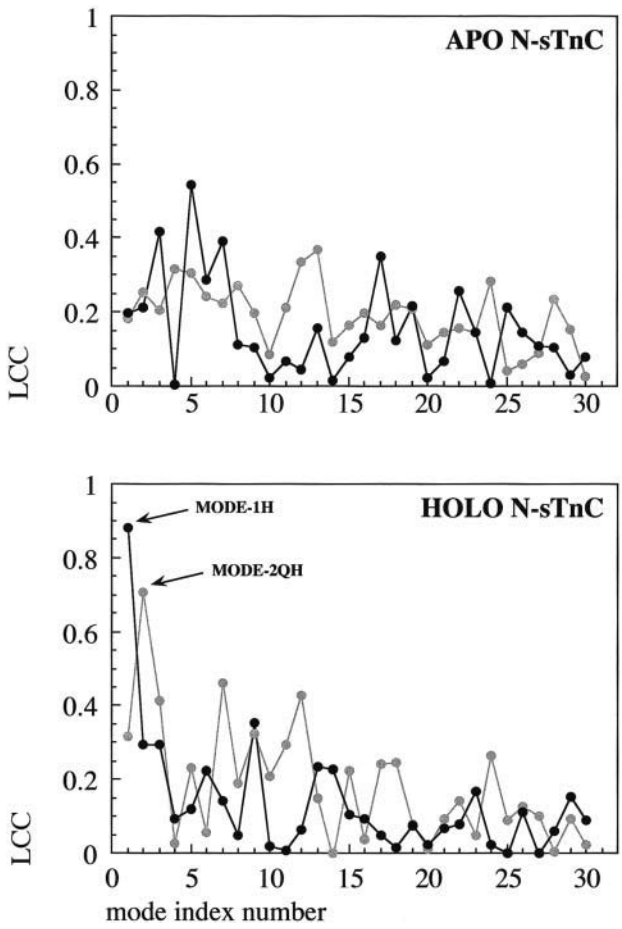

FIGURE 5 Coefficients of linear correlation between the structural deformations produced by each dominant harmonic (*solid*) and QH (*shaded*) mode and the experimentally observed Ca^{2+}-induced changes. Only absolute values are shown, because the sign of the coefficients is conventional, reflecting the direction of motion produced by the modes.

search was that the direction of the modes relates to the transition path and, therefore similar mechanisms would determine the observed conformational changes.

A precise description of the motion due to modes-1H and -2QH was given by the Cartesian components of the corresponding eigenvectors from vibrational analysis. The eigenvectors are 3N-dimensional quantities, with x-, y-, and z-components for each protein atom. Vectorial components were calculated from the generic term in Eq. 3 using the amplitude and frequency for each of modes-1H and -2QH. The histograms in Fig. 7 *a* show that the modes describe similar motions, with large displacements along the x and y axes. The large amplitude motion in the (x, y)- plane involves two main structural blocks: residues 42–60 (partial helices (B, C) and the linker) and the group of residues 18-25/77-86 (helices (A, D). To include longer α-helical segments in the defined structural blocks, the cutoff criterion in Fig. 7 *a* was adjusted to comprise residues with smaller displacements and the same directionality as the rest of the block. The motion also affects other elements of the structure, e.g., the two Ca^{2+}-binding loops and helix Nt that move in concert with helices (A, D) along the x- and y-direction, respectively.

The structural effect of modes-1H and -2QH is illustrated in Fig. 7 *b* by projecting the x- and y-components of the corresponding eigenvector onto the molecular model of the protein. The blue segments indicate positive components for residues 42-60 of helices (B, C) and of the adjoining linker. Helices A and D are either invariant to the motion or move in the negative direction of the axes. The movement of residues 42-60 in the direction of the x axis produces an upward displacement relative to the (y, z)-plane, which brings them

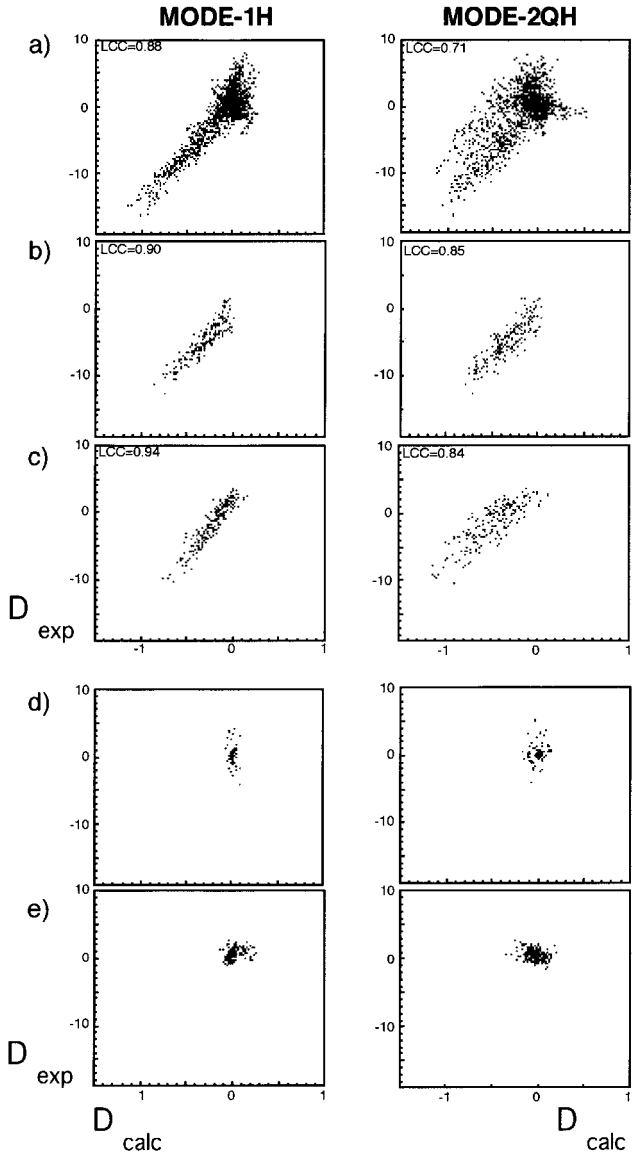

FIGURE 6 Relationship between the structural changes produced by modes-1H and -2QH of holo N-sTnC, and those observed experimentally in the holo→apo transition. Calculated and experimental values are expressed as components of the generalized vectors D_{calc} and D_{exp}, respectively (see text). The two vertical panels illustrate correlations between the components of D_{calc} and D_{exp} for each of modes-1H and -2QH. The data include various selections: (*a*) all components of the vectors; (*b, c*) components from the displacements of helices B and C relative to the (Nt, A, D) group of helices, respectively; (*d, e*) components from relative displacements within the groups of helices (B, C) and (Nt, A, D), respectively. All values are expressed in Å. Correlation coefficients were not estimated for the cluster of small values in plots *d* and *e*.

closer to helices (A, D). This net movement toward helices (A, D) is the resultant of individual motions, in which residues 42-60 have larger positive components (Fig. 7 *a*). The motion of the two structural groups in opposite directions along the *y* axis also favors a decrease in the separation distance.

The results for holo N-sTnC indicate a molecular mechanism in which residues 42-60 move toward helices (A, D), in a direction that brings them closer to the hydrophobic surface of the helices. Consistent with the experimental description of a closing conformational change for N-sTnC, our calculations yield evidence on the directionality of the motions involved in the holo→apo transition. However, a direct comparison of these findings with the experiment was not yet feasible due to the lack of appropriate empirical measures for the dynamics of the transition.

Proposed autoinhibitory role for helix B and adjacent linker residues

We noticed that the movement of residues 42-60 toward helices (A, D) describes a mode of binding of the mobile segment to the surface used by the protein to interact with its target, TnI. To characterize the binding mode, we sought to identify potential interactions formed by residues 42-60 at the binding interface during the vibrational motion produced by modes-1H and -2QH.

The structural deformation that favors a proximal position of these residues relative to the binding surface could be attained at the amplitude of vibration. However, for a vibrational motion of energy k_bT, the largest displacements of 0.7 Å from the reference, holo structure (Fig. 7 *a*) are still too small to achieve such a location. This limitation to small deviations from equilibrium is inherent to the harmonic approximation used to calculate the modes. A possible approach to overcome this limit is to scale up the structural changes produced by modes-1H and -2QH. To achieve contact distances between residues 42-60 and the interactive groups, the atomic displacements must be augmented almost ten times. However, linear extrapolation beyond the limitations of the model is a controversial approach because it may yield unphysical distortions to the system. To prevent such artifacts and still bypass the restricted conformational sampling performed by the modes, we chose to analyze the apo state of the protein, as a physically relevant state located along the direction of modes-1H and -2QH. This choice reconciles the main arguments of the above reasoning, and provides a structural frame for accurate analysis of the interactions formed by residues 42-60 at the target-binding surface.

The interactions between residues 42-60 and the rest of the protein were further characterized from the intramolecular contacts specific for the apo state (Table 1 *a*). Potential interactions at the target-binding surface were identified from the list of close contacts, by selecting those to residues that bind TnI. The definition of interactive residues relied on spectroscopic data for the complex between N-sTnC and a peptide fragment from TnI (McKay et al., 1997). Our results show that only the subset of residues 42-51 form close

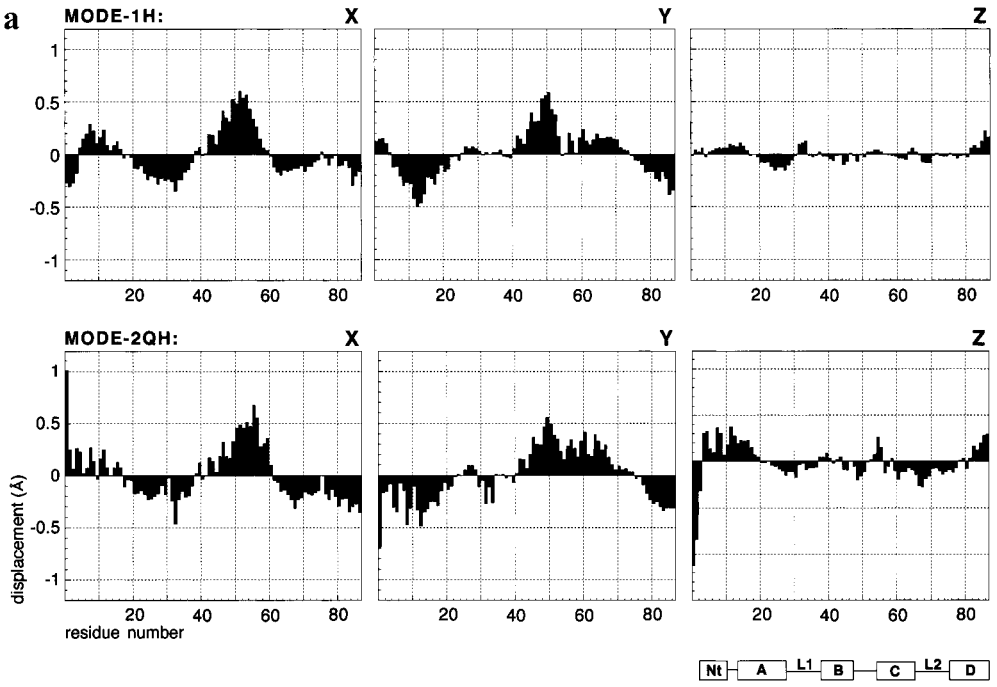

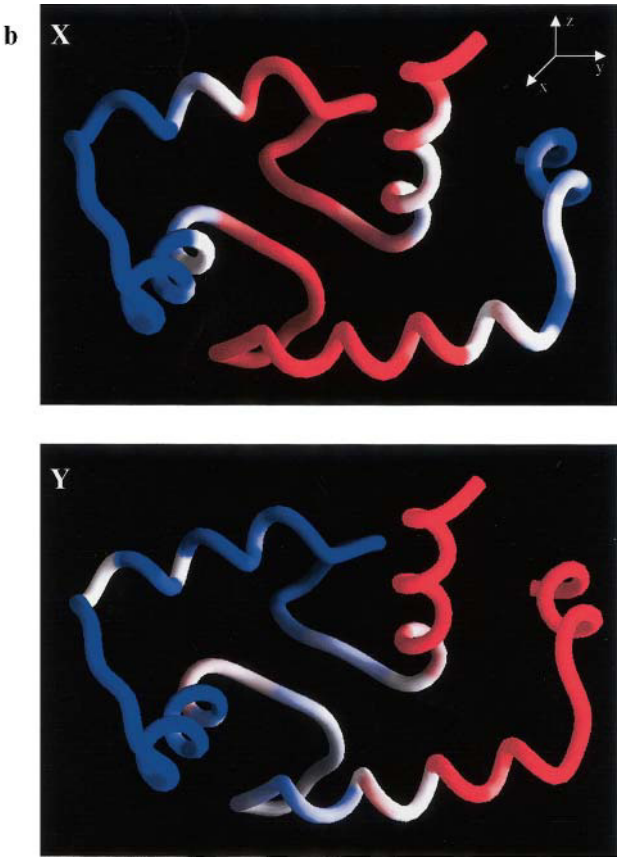

FIGURE 7 (*a*) Cartesian components of the atomic displacements produced by modes-1H and -2QH of holo N-sTnC. Displacements calculated for the C_α-atoms correspond to a total vibrational energy of the mode of k_bT and are expressed in Å. The direction of vibration chosen to illustrate the results leads to structural changes toward the apo conformation. The following groups of residues have positive (+) and negative (−) components larger than 0.07 Å. **Ox:** (+) 6-16/43-58 and (−) 21-38/62-74/81-87 (Mode-1H); (+) 43-61 and (−) 18-38/64-87 (Mode-2QH); **Oy:** (+) 42-71 and (−) 6-22/78-87 (Mode-1H), (+) 42-73 and (−) 1-22/78-87 (Mode-2QH); **Oz:** (+) 12-16/83-87 and (−) 21-29 (Mode-1H), (+) 4-19/83-87 and (−) 26-36 (Mode-2QH). Structural blocks comprise at least four consecutive residues. Large blocks may include up to two successive residues of components below the cutoff and of same directionality as the rest of the block. (*b*) Ribbon diagram of holo N-sTnC colored according to the x- and *y*-displacements produced by mode-1H. To illustrate rigid-body motions that involve atoms with displacements larger than the 0.07 Å cutoff, the color code intervals are: red→white for negative values ≤ -0.15 Å and white→blue for positive values ≥ 0.15 Å. Light zones correspond to groups of atoms invariant to the vibration, within the chosen cutoff criterion. The molecule is viewed from the (*y*, *z*)- plane, tangent to the interaction surface (see Methods). Atomic coordinates from the crystal structure of holo N-sTnC (Strynadka et al., 1997) do not include values for the disordered residues 1-6.

interactions at the target-binding surface. The interactions are mostly hydrophobic, with contributions from helices (A, D), of which the aromatic cluster of Phe-22, -29, and -78 is involved in the most numerous contacts. From the observed network of intramolecular interactions, it results that, in the apo state of the protein, residues 42-51 are actually bound to the interactive surface.

Under the assumption that the apo state is representative

TABLE 1 Close contacts formed by residues 42-60 of N-sTnC (*a*) and by a peptide fragment from TnI (*b*), in the apo and in the complexed state of the protein, respectively

a		b	
Residues 42-60	apo	Peptide	Complex
L42	16M*†	S117	A24*
	173*	A118	—
	F78*	D119	—
G43	—	A120	F29*†
T44	F29*†		M82*†
	E41	M121	A25*†
V45	E29*†		M28*
	I37*		F29*†
	F78*		V45*†
M46	L58	L122	—
	Q85		
R47	N52	K123	—
	P53	A124	F29*†
	L58		M82*†
M48		L125	F29*†
	F29*†		E12*†
			M45*†
L49	F22*		M46*†
	A25*†		
	F78*		
G50	—		
Q51	M82*†		
	Q85		
	M86*		
N52	R47		
P53	R47		
	E57		
	E58		
T54	E56		
	E57		
K55	—		
E56	T54		
E57	P53		
	T54		
	Q85		
L58	M46*†		
	R47		
	P53		
D59	—		
A60	—		

Hydrophobic residues at the interaction surface of N-sTnC are marked with an asterisk, and an additional dagger indicates groups shown by NMR spectroscopy to have altered chemical environments upon binding fragment 117-125 of Tnl (McKay et al., 1997). Molecular contacts were counted for side chain atoms within 4 Å. Atomic coordinates were obtained from the crystal structure of apo N-sTnC (Herzberg and James, 1988), and from the molecular model built for the complex with the TnI fragment (Fig. 8 *b*).

for the structural changes produced by modes-1H and -2QH, we considered that results are transferable for the characterization of the modes. The movement of residues 42-51 toward helices (A, D) during the vibration due to modes-1H and -2QH was, therefore, found to describe a mode of binding to the surface used by the protein to interact with TnI. By competing for the same binding surface, the mobile region, comprising helix B and adjacent linker residues, could block the access of TnI to residues critical for the formation of the complex. Because the inhibition is internal, we propose that residues 42-51 play an autoinhibitory structural role, by obstructing the access of the target to the interaction surface. This assumption could be pivotal in coupling the two functions of N-sTnC: the response to Ca^{2+} and binding to TnI.

Peptide mimetics as a principle for autoinhibition

To identify the basis for autoinhibition in the structural action of residues 42-51, we further pursued comparative analysis for two states of N-sTnC, which pose different molecular contexts at the target-binding surface. The chosen states differ in the nature of the peptide segments bound to the interaction surface: the autoinhibitory region, for the apo protein, and a fragment from TnI, for the TnC-TnI complex. From structural comparison, we sought to characterize the mode of binding of the peptides and the matching contacts at the binding interface.

Results discussed in the preceding section showed that the vibrational motion due to modes-1H and -2QH favors binding of residues 42-51 to the target-binding surface. The molecular contacts attainable in the extrapolation beyond harmonic structural changes are included in Table 1 *a*. The corresponding graphic representation of the autoinhibitory region illustrates its occluding location relative to critical interactive residues, as the aromatic cluster of Phe-22, -29, and -78 (Fig. 8 *a*).

The second system for analysis was a molecular model of the complex between holo N-sTnC and a peptide fragment from TnI, comprising residues 117-125. The modeling protocol was chosen to meet two main requirements: 1) to use a highly homologous template, i.e., the N-terminal domain of calmodulin (CaM) complexed with a peptide fragment from kinaseIIα (Meador et al., 1993); and 2) to include most interactions observed spectroscopically for the TnC-TnI complex (McKay et al., 1997). In a similar reference frame as for apo N-sTnC, Fig. 8 *b* shows the position of the TnI fragment relative to the aromatic cluster at the binding surface. A complete account of the molecular interactions involved is given by the list of close contacts in Table 1 *b*.

The molecular representations in Fig. 8 indicate similar modes of binding of the autoinhibitory region and of the TnI fragment to the interaction surface. As illustrated by their location at the binding surface, the peptide segments form numerous contacts to the aromatic residues Phe-22, -29, and -78. From the observed patterns of interaction, we derived the following sequence alignment of the peptides

$$\begin{aligned} &\text{autoinhibitory region: } {}^{42}\mathbf{L}\,\mathrm{G}\,\mathrm{T}\,\mathbf{V}\,\mathbf{M}\,\mathit{R}\,\mathrm{M}\,\mathbf{L}^{(50)} \\ &-\text{TnI peptide: } {}^{125}\mathbf{L}\,\mathrm{A}\,\mathit{K}\,\mathbf{L}\,\mathbf{M}\,\mathrm{A}\,\mathrm{D}\,\mathbf{A}^{(117)}. \end{aligned} \tag{13}$$

The binding motif comprises hydrophobic residues with $(i, i + 3)$ or $(i, i + 4)$ periodicity and basic amino acids at

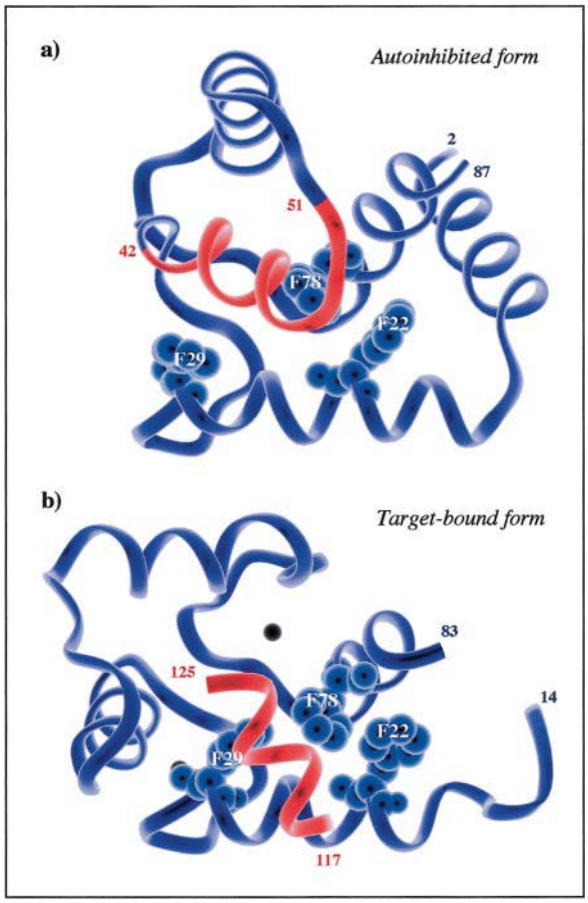

FIGURE 8 Illustration of the mode of binding the autoinhibitory structural element (*a*) and a peptide fragment from TnI (*b*) to the interaction surface of N-sTnC. (*a*) Crystal structure of apo N-sTnC (Herzberg and James, 1988). The autoinhibitory region (*red*) comprises residues 42-51 of helix B and of the adjacent linker. Aromatic residues which mark the site of interaction are shown in an all-atom representation. (*b*) Model complex of holo N-sTnC with a peptide fragment from TnI (residues 117-125). The complex was built using the modeling program MODELLER (Sali et al., 1997). The protein and the peptide were built by analogy to the crystal complex of CaM with a peptide fragment from kinaseIIα (Meador et al., 1993). The following template/target alignments were used for modeling: residues 4-73/14-83 for the protein and residues 301-309/117-125 for the peptide. The complex was assembled by superimposing each component onto the corresponding atoms of the template: rms deviations of C_α-atoms are 1.0 Å and 0.6 Å for the protein and peptide, respectively. Steric clashes at the binding interface were relieved by minimization for 100 steps of steepest descents and 100 steps of conjugate gradient method. The N-terminal helix of N-sTnC is absent in the model because it had no equivalent template in CaM.

either terminus. The inverse orientation of the peptides is likely to reflect the structural constraints on the autoinhibitory region, which is an internal structural unit of the protein. Let it also be noted that differences observed in binding the two peptides are related to the dual role of helix B, which is either bound to or is part of the interaction surface.

The structural similarities observed in binding the autoinhibitory region and the TnI fragment indicate that target mimetics could form the basis for autoinhibition. By competing for the same interaction surface, the autoinhibitory segment mimics target binding and can block the access of the TnI fragment to interactive residues.

Functional role of methionines at the interaction surface

The adaptation of the protein structure during the holo→apo transition marks the structural response of N-sTnC to the Ca^{2+} signal that triggers its regulatory function. Structural adaptation involves changes in the relative position of the groups of helices (B, C) and (Nt, A, D) to a closed, apo conformation. In terms of the autoinhibition model, such rearrangements imply binding of helix B and of adjacent linker residues to the surface used by the protein to interact with TnI. We, therefore thought to identify side chain properties at the interaction surface of holo N-sTnC that mediate the molecular interactions for adaptation in the transition.

The dynamic and structural attributes of these residues were further characterized using conventional methods for analysis of the simulations. The trajectory interval for analysis included the last 400 ps of the run, and it was selected according to criteria for structural stability (see Appendix).

Methionines form a smooth shield

The dynamics of protein side chains at the interaction surface was first assessed from the distribution of the atomic fluctuations. The data used for illustration was derived from the simulation of holo N-sTnC and it was validated in the appended section for results by comparison to x-ray thermal factors. Our findings indicate an asymmetric distribution of the fluctuations, with high values at the interactive face of the protein (Fig. 9). This region includes mostly hydrophobic residues, i.e., seven methionines, Leu-49, Phe-13, and Phe-29. Although the side chains of methionines are intrinsically flexible due to the rotational freedom around the χ_3 torsion angle (Gellman, 1991), Leu-49 undergoes global movements characteristic for the unrestrained linker between EF-hand motifs. The high mobility of Phe-13 and Phe-29 is due to flips of the aromatic rings favored by weak interactions with nearby residues and by their partial exposure to the solvent.

We further noticed that the cluster of methionines is located over other interactive hydrophobic residues, forming an outer layer for target encounter. This topology favors an occluding position for the long side chains of Met residues. To assess the extent by which methionines obstruct other interactive residues, we compared the surface accessibility of these residues in the native protein and in single Met→Ala mutants (Table 2). The mutants were designed to reveal occluded surfaces by systematically excluding the side chain of each methionine. Results show that methionines partially

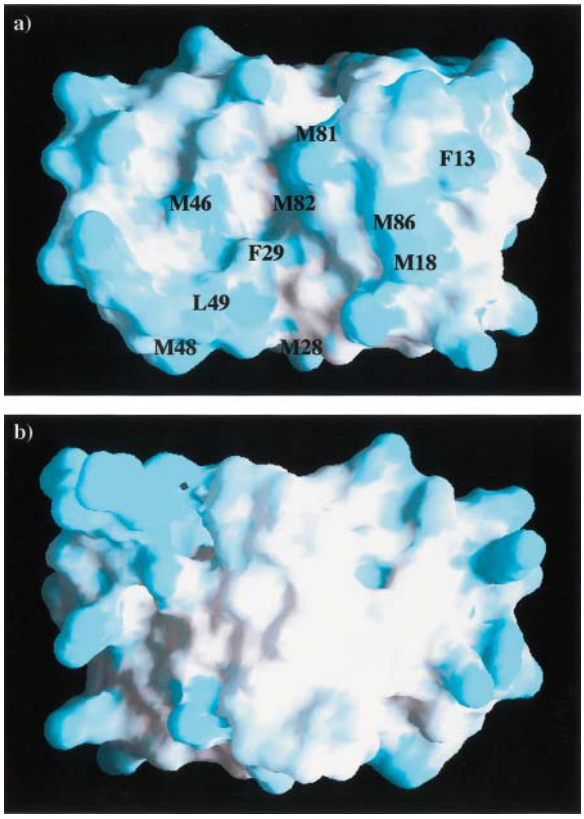

FIGURE 9 Molecular surface of holo N-sTnC colored according to temperature factors from the MD simulation. Each panel illustrates a view of the protein from (*a*) the interaction surface and (*b*) the opposite face. Colors white→blue were gradually assigned to values within the range [15, 40] Å^2. Labels indicate highly mobile hydrophobic residues at the interaction surface. The molecular surface was calculated for the average structure from states sampled in the last 400 ps of simulation.

TABLE 2 Surface area calculations probing the occluding role of methionines at the interaction surface of holo N-sTnC

	Native	M18A	M86A	M82A	M81A	M46A
Phe-29	31.4	—	—	—	—	37.0
Phe-22	24.5	31.2	31.8	36.7	—	—
Leu-79	8.8	—	—	—	—	—
Phe-78	11.2	—	—	24.7	20.4	—
Ile-73	3.6	—	—	—	5.9	—
Val-65	8.9	—	—	—	25.0	—
Ile-62	3.5	—	—	—	—	22.4
Leu-42	8.9		—	—	—	—
Ile-37	0.8					
Val-45	10.0					

The accessibility of interactive residues to external probes was determined for the native protein and for single Met→Ala mutants (probe radius = 1.4 Å). Underlined values indicate changes larger than 5% of the corresponding side-chain surface area, whereas dashes mark surface areas invariant to the mutations. Mutations of Met-28 and Met-48 were not included because of negligible effects. The sites of mutation were ordered according to the location at the interaction surface, counted couterclockwise to the view in Fig. 9. Atomic coordinates for the native protein were obtained by averaging over states sampled in the 400 ps of production run.

shield interactive hydrophobic residues, which are otherwise secluded from the solvent. The largest structural effect was observed for the aromatic moieties of Phe-22 and Phe-78, for Leu-42, and for Val-65.

This observation from simple visual inspection of the structure of holo N-sTnC prompted the following interpretation of our findings. It is proposed that methionines form a smooth shield, easily removable to increase the exposure of other interactive hydrophobic residues. The energetically inexpensive rearrangement at the interaction surface should uncover Phe residues and other hydrophobic residues for favorable interactions with the potential target. The energy cost for such changes is small, due to the high flexibility of the occluding Met side chains, and to their weak interaction with the shielded hydrophobic residues. It is recalled that in the autoinhibition model for the holo→apo transition, the target is internal, formed of helix B and of adjacent linker residues.

The proposed structural role of methionines is consistent with experimental data showing a large involvement of otherwise secluded hydrophobic residues to the formation of the apo state (Herzberg and James, 1988). These residues could have become available for interaction with the autoinhibitory region only upon displacing the methionines from their occluding position at the interaction surface. The observed displacements range from very large values, for Met-46 and Met-48, to small, local rearrangements, for Met-81 and Met-82 (Herzberg and James, 1988; Strynadka et al., 1997).

CONCLUSIONS AND DISCUSSION

The underlying hypothesis tested in this work is that the regulatory domain of sTnC features intrinsic motions related to the transition between open and closed conformations. Results from NM and QH analyses showed that only the Ca^{2+}-bound form of the domain undergoes a slow vibration along specific modes in the direction of the transition. The vibrational motion produces distorsions of the open structure toward the closed form, in which the helices adopt a more compact arrangement. Such effects are of interest because they occur in the low-frequency regime and, therefore, yield dominant contributions to the global fold of the protein. Characteristic for the Ca^{2+}-sensing action of N-sTnC, these structural changes are enhanced upon releasing the cation at the low affinity binding site. An energetically costly process, the structural adaptation for transition is thus favored intrinsically, by preferential displacements of the groups of helices (A, D) and (B, C). It is noteworthy that our descriptions of the relationship between intrinsic and induced structural properties were established quantitatively, in good agreement with the experiment.

The analysis of the vibrational motions relevant for transition is an important step in understanding at molecular level the observed large changes between open and closed

conformations. From the calculated atomic contributions to the modes specific for the holo state, it was possible to extract a detailed characterization of the motions and mechanisms involved in the process. Let it be noted that the structural effect of the modes was assessed from motions in the direction of vibration leading to a closed state. Vibrations in the opposite direction produce changes that further open the structure, and enlarge the hydrophobic surface presented for molecular interaction. A possible relationship to target binding was presented elsewhere for the C-terminal domain of CaM, a related system of the EF-hand family of modulatory Ca^{2+}-binding proteins (Pitici, 1999). Modes-1H and -2QH of holo N-sTnC were thus found to produce a movement of helices (B, C) and of the connecting linker toward helices (A, D), in a manner that resembles binding to the interaction surface. Structural data were consistent with our proposal that the subset of residues 42-51, comprising helix B and adjacent linker residues, plays an autoinhibitory structural role. By competing for the same binding surface as the TnI target, these residues block the access to hydrophobic groups critical for the formation of the complex. The sequence and structural similarities between this element of the structure and the binding region of TnI further indicated that the principle for autoinhibition is target mimetics, a prescript often used by biomolecular systems to modulate function.

In this representation, the conformational transition to a closed form is viewed as an association between the autoinhibitory region and the rest of the protein. The process involves binding of helix B and of adjacent linker residues to the surface used to interact with TnI. Target binding is therefore, a competitive event, which engages similar hydrophobic groups for interaction. We further discuss the implications of the proposed autoinhibition model for transition, in relationship to the Ca^{2+}-sensing function of our prototype system. The reasoning concerns two contributions to the equilibrium between apo and holo states: the intrinsic binding affinity of the autoinhibitory region, and the perturbation induced by target molecules.

Although not amenable for direct experimental determination, the first component is implicitly included in the measure for Ca^{2+}-binding affinity. High intrinsic affinity of the autoinhibitory region for the interaction surface favors the closed conformation characteristic of the apo state, and therefore, corresponds to low Ca^{2+}-binding affinity. The involvement of residues 42-51 in the process can be assessed using various selection criteria for mutagenesis. A direct combinatorial approach involves systematic changes that may, for example, be sorted to preserve the residue type at each location. We propose to refine the selection using our finding that helix B and the adjacent linker residues mimic target binding at the interaction surface. Mutations can thus be designed by analogy to the binding region of TnI, or to various peptide fragments that also bind CaM, a closely related modulatory protein. An alternative option is to choose mutations by homology to the autoinhibitory region of other Ca^{2+}-binding proteins of the EF-hand family. The intrinsic binding affinity of residues 42-51 could, in principle, be tuned to yield constitutively active or inactive constructs that are not sensitive to Ca^{2+}, but adopt open and closed conformations, respectively. We note that a closed construct has been obtained so far only by covalently linking reduced cysteins at position 46 and 82 of the regulatory domain of sTnC (Grabarek et al., 1990). Some residues to be first targeted by mutations are: Val-45 and Leu-49, which form the most numerous contacts with helices (A, D) in the closed form, and Arg-47, the single basic residue of helix B. (The two conformations accessed in the Ca^{2+}-induced transition are nominated open and closed, for either wild-type or mutated systems. It is however noted that mutations can alter both conformations, producing, for example, less open or less closed structures. Open and closed forms were herein associated with the holo and apo states, respectively.)

Another contribution to the equilibrium between apo and holo states includes perturbation effects due to the interaction with target molecules. According to our model for transition, such effects arise from competitive binding of the targets to hydrophobic groups required to interact with the autoinhibitory region in the apo state. For low relative binding affinities, the targets have minor effects on the equilibrium, established intrinsically from intramolecular properties. However, for higher affinities, the targets bind to the interaction surface and hinder autoinhibition, hence favoring an open conformation and a higher affinity for Ca^{2+}. The principles for tuning Ca^{2+}-binding can be investigated using peptide fragments analogous to the autoinhibitory region of N-sTnC, or to corresponding segments from related proteins, as cardiac TnC or CaM. The peptides could also resemble target molecules specific for other proteins of the EF-hand family.

Interestingly, this discussion is consistent with biochemical assays for CaM which have characterized target-induced effects on Ca^{2+} binding (Peersen et al., 1997). Although in a different conceptual scheme, it has been shown that interactions with five different targets tailor Ca^{2+} binding to individual domains over a broad range of concentrations. It has also been proposed that intermolecular tuning of the Ca^{2+}-dependent response is a functional attribute of CaM, required to modulate signal transduction in various pathways.

Our proposal that the autoinhibitory region acts as a target mimic provides a theoretical framework for new questions regarding the relationship between Ca^{2+} binding and target binding. In the above comments, we suggested to tune Ca^{2+}-binding affinities intrinsically by changing the autoinhibitory region to incorporate groups specific for target molecules. Conversely, binding assays could probe the affinity of peptide fragments devised by analogy to the region used for autoinhibition. Chimeric constructs between the protein and targets might be also used to design Ca^{2+} sensors that have learned the role of helix B and of the adjacent linker as

a target mimic. It is noted that the idea of using EF-hand proteins as model systems for Ca^{2+} sensors has been explored so far for CaM (Porumb et al., 1994; Vukasinovic et al., 1997). However, the underlying concepts required to tune Ca^{2+} affinity are still intriguing and open for future study. We hope that the proposed dual functional role of helix B and of the adjacent linker would bring up a different perspective on the subject.

From the analysis of the vibrational modes, we found global properties related to the adaptability of the protein structure in the holo→apo transition. Such results form the basis for future investigations aimed at identifying computationally the structural link between Ca^{2+} binding and the conformational transition. A possible approach that combines analyses of the experimental structures and of the calculated modes is illustrated herein for Phe-29, a residue important for the Ca^{2+}-sensing function of N-sTnC (Li et al., 1995; Yu et al., 1999). It is nevertheless, beyond the scope of this work to pursue a thorough study on the subject, and to validate some related speculative comments.

We first notice the rearrangement of the protein core in the transition to the closed conformation, by which Phe-29 moves away and its separation from Phe-78 increases by almost 4 Å. This change reflects the intercalation of Val-45 between the two phenyl rings, as a result of the rigid body encounter between helix B and the aromatic cluster at the interaction surface. Initiated by small deformations due to modes-1H and -2QH, the intramolecular process of binding involves gradual displacements of the autoinhibitory region toward the interaction surface. The insertion of Val-45 occurs therefore, progressively, and it produces a lateral shift of Phe-29, which disrupts the interaction with Phe-78. An indication that the structural properties of Phe-29 are sensitive to movements of helix B was obtained from the analysis of modes-1H and -2QH (data not shown). The vibrational motion produced a marked decrease in the exposure of the aromatic ring, as a direct result of the occluding action of the displaced helix B. It is noted that a simple comparison of surface areas for the holo and apo states was not informative in this respect, because the aromatic moiety adopts different positions at the interaction surface.

Besides its interactions with the protein core and with the autoinhibitory region, Phe-29 is also tightly packed against residues of the EF-hand loop, at the junction between helices (A, B). Adjacent to the first Ca^{2+} ligand of the binding loop, Phe-29 could be a fine sensor of the Ca^{2+} signal by coupling local structural changes to global rearrangements of the domain. We suggest a possible coupling mechanism, in which Phe-29 acts as an adaptable wedge at the junction between helices (A, B), in direct relationship to the degree of opening of helix B relative to the interaction surface. The transition to the closed form involves a diminished wedge action of Phe-29, which is displaced from the junction by the closing helix B.

Such a structural role implies a critical dependence of the coupling mechanism on the size of the residue at this position. Smaller residues are likely to be less effective wedges that also favor a partial opening of the structure in the holo state. Various hydrophobic substitutions of Phe-29 could probe this assumption by altering side-chain packing at the junction between helices (A, B). A first, speculative expectation is that the degree of opening of the structure is proportional to the size of the residue at the wedge position. The relationship is however likely to be more complex because Phe-29 interacts with aromatic residues of the protein core, in direct determination of the protein stability. Additional studies will nevertheless, be pursued to probe computationally the proposed wedge action of Phe-29 in the transition.

Two sets of experimental data have indicated the sensitivity of the Ca^{2+}-induced response to substitutions of the phenylalanines preceding the first Ca^{2+} ligand of the binding loops. Apparently conservative, the Phe→Trp mutation at position 29 of N-sTnC affects the Ca^{2+}-binding properties by perturbing both the apo and the holo states (Li et al., 1995; Yu et al., 1999). Until better characterized structurally, it is noted that, the apo form of the mutant features altered packing and dynamics of the core residues Phe-26 and Phe-75. Earlier studies of CaM have also shown that the analogous F92A construct is less effective in coupling Ca^{2+} binding to the structural changes (Ohya and Botstein, 1994; Meyer et al., 1996). The observed higher Ca^{2+} affinity reflects the reduced stability of the apo state due to disrupted packing within the EF-hand motif, and to more favorable solvation of the partially open holo structure.

As already noted, we identified from the vibrational modes molecular mechanisms related to the structural adaptation of N-sTnC in the holo→apo transition. Described as a closing of the domain, the adaptation involves binding of helix B and of adjacent linker residues to the surface used by the protein to interact with TnI. The plasticity of the interaction surface was therefore, expected to be an important element for recognition in this process of intramolecular association. To assess such contributions to binding, we also characterized the side chain properties of holo N-sTnC using conventional methods for structural analysis.

Results indicated a specific molecular pattern at the interaction surface, by which methionines are clustered over other hydrophobic residues and delineate a sparse outer layer. We propose that Met side chains are easily removable to increase the accessibility of more secluded residues, as Phe-29, Leu-42, Val-65, and Phe-78, to favorable interactions with the autoinhibitory region. Energetically inexpensive, such rearrangements are made possible by the high intrinsic flexibility of the occluding methionines, and by the weak molecular interactions involved.

This structural role is also related to the solvation properties of the amino acids at the interaction surface. Due to their high solubility (Wimley et al., 1996), methionines could optimize the solvation of large hydrophobic surfaces (Nelson and

Chazin, 1998). We point out a potential large contribution to solvation by specific groups of interacting Met-Phe residues, whereby the sulfur atoms are close to the δ-hydrogens of the aromatic rings. The quantum-mechanical origin of this interaction has not been yet characterized, but its occurrence in various molecular systems (Thomas et al., 1982) appears related to the higher polarizability of sulfur relative to carbon (Fersht, 1985). The combined structural and interactive properties of methionines thus provide an effective mode of presenting to molecular encounter an interaction surface rich in phenylalanines.

Because N-sTnC uses the same surface to interact with TnI, the above discussion pertains as well to the process of protein-target association. The participation of methionines in the formation of the complex has been assessed spectroscopically from the changes in chemical shifts and/or intermolecular nuclear Overhauser effects (McKay et al., 1997). However, the functional implication of side chain flexibility and interactivity at the binding surface has not yet been addressed systematically. Results for CaM, which features a similar mode of binding target molecules, have been so far consistent with a plastic nature of the binding surfaces rich in Met residues (Zhang et al., 1994; Vogel and Zhang, 1995). The interpretation of the binding and activation assays can now be sought in a specific manner, in relationship to the occluding and interactive role of methionines.

The procedure illustrated for the regulatory domain of sTnC can be further utilized to identify the structural and dynamic basis for functional differences among proteins of the EF-hand family. Applications to the C-terminal domain of CaM, for example, revealed specific properties, which relate to the experimentally observed Ca^{2+}-dependent phenotype (Pitici, 1999, 2001). Irrespective of the Ca^{2+} occupancy, the domain had no intrinsic propensity for changes between open and closed structures. Consistent with a transition mechanism that involves multiple intermediates in conformational exchange (Evenas et al., 1999), these findings provided additional support for our methodological approach. Current work is aimed at understanding the molecular determinants for the Ca^{2+}-induced response of cardiac N-TnC, the isoform that requires only one Ca^{2+} for function. Mechanistic differences will be treated using the newly proposed concepts of autoinhibition and target mimetics.

Further studies are also needed to clarify the role of Ca^{2+} in triggering conformational changes in the direction of a specific vibrational mode. We established a relational statement by which the intrinsic structural variations due to slow vibrations are similar to those observed experimentally in the Ca^{2+}-induced transition. However, the physical basis for this relationship is not yet clear, because no method of experimentation has clarified the nature of the interactions involved and the dynamics of transition. Let note that this issue pertains as well to other systems in which similar correlations have been found between intrinsic motions and biological functions, as enzymatic activity (Brooks and Karplus, 1985) or fiber polymerization (Tirion and ben-Avraham, 1993). Could the paucity of data reflect a methodological impasse, especially that, for N-sTnC, the pattern of Ca^{2+} ligation has been characterized at high resolution, and has revealed the potential interactions? We have made a first attempt to incorporate perturbation effects in a linear response theory by modeling the cations as small Ca^{2+}-like particles (Pitici, 1999). Although not yet explaining the role of Ca^{2+} on specific vibrational modes, preliminary results have indicated higher sensitivity for structural changes in the direction of the transition. The following questions could be further addressed with respect to this subject: Does the cation act by simply enhancing the small oscillations of an existing mode, thus supplying energy into one degree of freedom? Or does it couple the intrinsic vibrations into a resultant motion along the transition path? What is then the relationship with the intrinsic mode pointing in the direction of the conformational transition?

APPENDIX: QUALITY OF THE MD SIMULATIONS

Standard analysis was carried out to assess the quality of the MD simulations used to calculate QH vibrational modes. The requisite for accuracy stems

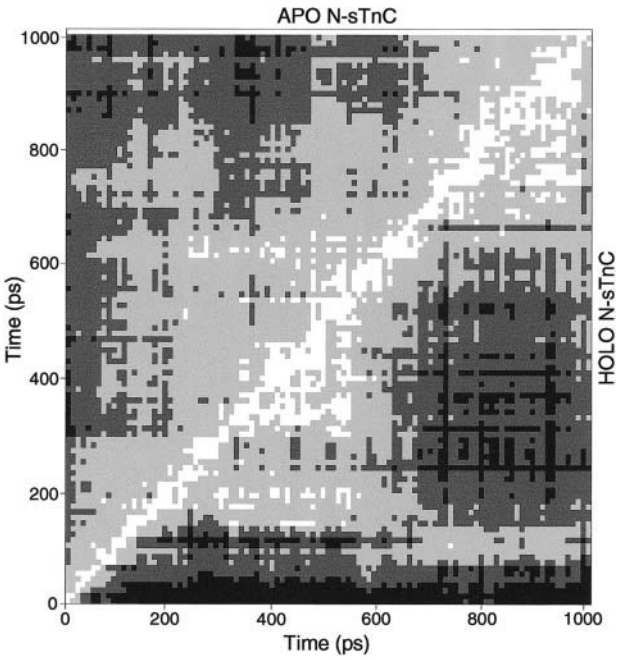

FIGURE 10 Matrix representation of the rms differences between conformational states sampled in the MD simulation of apo and holo N-sTnC (*upper and lower triangle, respectively*). Contours delineate families of structures chosen for analysis which correspond to the time intervals 719–1019 ps and 628–1028 ps, for apo and holo N-sTnC, respectively. Rms deviations from the starting structure for each of the apo and holo protein are 1.5 ± 0.2 Å and 2.0 ± 0.2 Å, respectively. Calculations include the C_α-atoms of residues 4: 84. Color code: rms ≤ 0.8 Å (*white*); 0.8 Å $<$ rms ≤ 1.2 Å (*light gray*); 1.2 Å $<$ rms ≤ 1.6 Å (*dark gray*); 1.6 Å $<$ rms ≤ 2.0 Å (*black*).

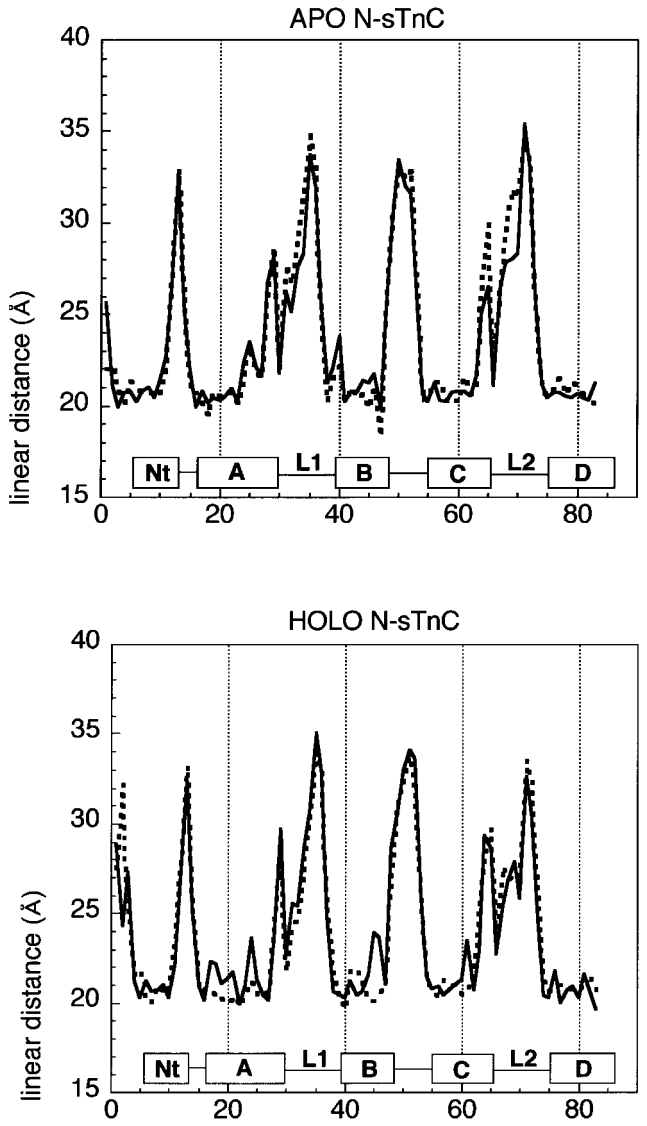

FIGURE 11 Linear distance values calculated for the starting structure (*solid line*) and for the last structure sampled in the simulations of apo and holo N-sTnC (*dotted line*). The linear distance for a four residue-long region with ideal α-helicity is 20.7 Å. Elements of secondary structure are defined from NMR spectroscopy (Gagne et al., 1995; Li et al., 1997).

from the formulation of the QH analysis, in which the force constant matrix is defined from fluctuations sampled with MD protocols (Eq. 5).

Energetic and structural properties were first monitored to ascertain the stability of each simulated system during the production run. Results from the simulations were further validated by comparison to experimental data. The comparison involved two descriptors of protein dynamics that have been well characterized empirically: the atomic fluctuations and the backbone ^{15}N order parameters.

Stability

Thermal and energetic properties of the simulated systems were found to be stable throughout the 1 ns-long production run. The last temperature scaling occurred within 40 ps of dynamics. During the production run, thermal fluctuations did not exceed 4 K, and the overall energy losses were less than 0.2‰ of the average total energy.

The gradual conformational changes of the proteins during the simulation were monitored by matrices of mutual rms deviations between trajectory frames (Fig. 10). Alternating light-dark patterns in the two-dimensional plots indicate structural fluctuations around average conformations. The large dark-colored block observed for apo N-sTnC represents structural relaxation in response to the removal of the packing interactions characteristic for the initial crystal structure (Herzberg and James, 1988). The rms maps were used to select the trajectory segments appropriate for analysis. The chosen ensembles include states sampled in the late part of each trajectory, and which have mutual rms values $\leq$1.2 Å.

Both the apo and the holo proteins retained essential structural properties that confer stability during the simulation. The backbone conformation was characterized using the Linear Distance Plot (Liebman et al., 1985), which cumulates the interatomic distances between reference backbone atoms and their nearest four neighbors. Results for states sampled at different instants of the run show that the elements of secondary structure were preserved until the end of the simulation (illustrated in Fig. 11 for the starting structure and for the last snapshot in the trajectory). It was observed that the irregularities of α-helical geometry present in the starting NMR structure of holo N-sTnC were corrected during the simulation. The short β-sheet that connects the EF-hand motifs is thought to be an important element of structural stability (Herzberg and James, 1988; Gagne et al., 1995). The β-sheet is primarily formed of two hydrogen bonds between Ile-37 and Ile-73, the residues at position 8 of each Ca^{2+}-binding loop. The apo conformation is stabilized by two additional hydrogen bonds between Gly-35 and Phe-75, and between Thr-39 and Gly-71 (Herzberg and James, 1988). The linear and dial plots in Fig. 12 show that the hydrogen bonds involved in the formation of the β-sheet maintain an ideal geometry throughout the simulation.

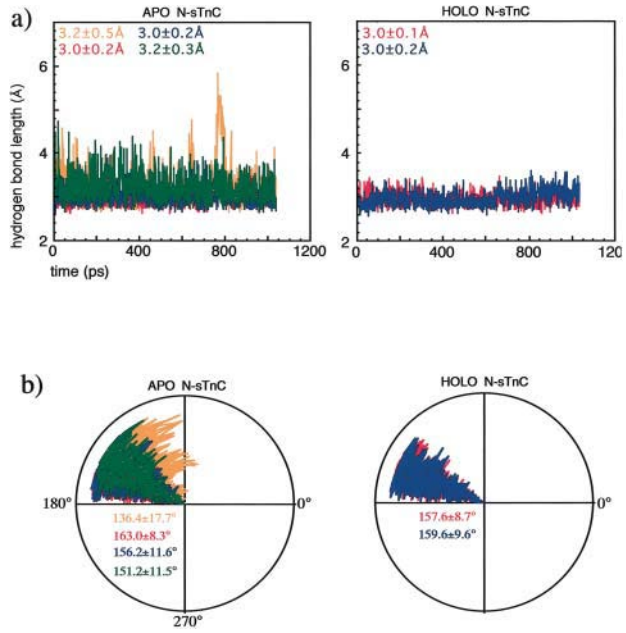

FIGURE 12 Time variation of the hydrogen bonds between Ca^{2+}-binding loops during the MD simulations of apo and holo N-sTnC. Local geometry is described by: (*a*) acceptor - hydrogen donor atom distances; and (*b*) planar angles formed by N: H: O atoms. The following hydrogen bonds were monitored during the production phase of the runs: Gly-35(O): Phe-75(N), Ile-37(N): Ile-73(O), Ile-37(O): Ile-73(N), and Thr-39(N): Gly-71(O). Atom definitions were color coded to match the figures, i.e. orange, red, blue, green. The marginal bonds involving Gly-35 and Thr-39 of the first β-strand are characteristic only for apo N-sTnC. For each hydrogen bond, plots include average linear and angular parameters, and the corresponding standard deviations from simulations.

Comparison to experimental data

Fluctuations

Often related to functional attributes of the biomolecular systems, the atomic fluctuations are amenable to both computational and experimental determination. It is, therefore an important validation test to compare the calculated rms fluctuations, $\sqrt{\langle(\Delta r_n)^2\rangle}$ (for each atom n), with those from the crystallographic B-factors (Eq. 10). The experimental values were obtained from the crystallographic refinements of apo and holo N-sTnC (Herzberg and James, 1988; Houdusse et al., 1997; Strynadka et al., 1997).

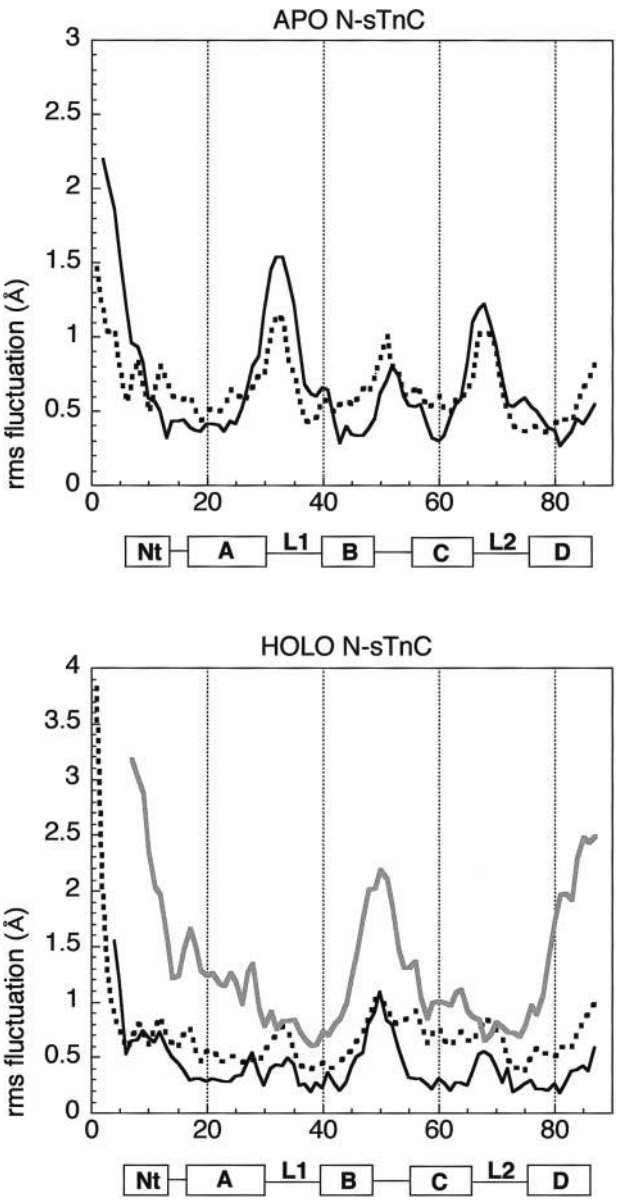

FIGURE 13 Comparison of backbone rms fluctuations from MD simulations (*dotted line*) and from crystallography (*solid lines*). Calculated values correspond to the trajectory intervals selected for analysis as shown in Fig. 10. Experimental fluctuations were obtained from the crystallographic B-factors of apo ((Herzberg and James, 1988) *black line*) and holo N-sTnC ((Strynadka et al., 1997) *black line*; (Houdusse et al., 1997) *gray line*). Elements of secondary structure were defined from NMR spectroscopy (Gagne et al., 1995; Li et al., 1997).

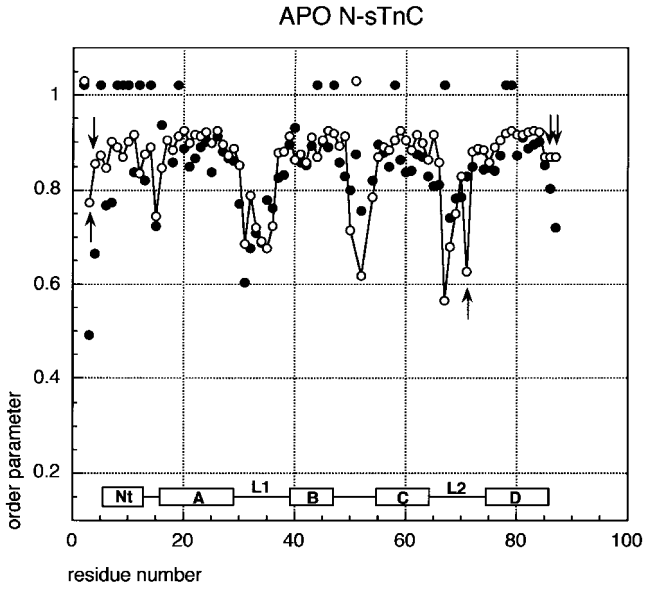

FIGURE 14 Computed (○) and experimental (●) backbone ^{15}N order parameters for apo N-sTnC. Markers above the $y = 1.0$ line indicate residues for which the calculation did not converge, and those for which no experimental value has been determined. Arrows indicate deviations larger than two standard deviations, i.e., 0.14 units, from the experiment.

Similar to results for other molecular systems (McCammon and Harvey, 1991), the computed rms fluctuations of protein backbone atoms were in good qualitative agreement with the x-ray data (Fig. 13). Systematically high values reported by Strynadka et al. for the holo protein (Strynadka et al., 1997) probably reflect a certain lattice disorder independent of intrinsic vibrations and/or the coupling between vibrations of a protein and its nearest neighbors due to tight packing (McCammon and Harvey, 1991).

A notable exception from the general trend was helix C of holo N-sTnC, with small relative fluctuations in the crystal, but high mobility in the simulation. Structural data by Houdusse et al. indicate that nonspecific binding of Ca^{2+} to Asp-56 and Glu-60 of helix C could account for the small relative fluctuations of helix C observed experimentally (Houdusse et al., 1997). Without such constraints in the simulated solution medium, the helix was more mobile, with average backbone rms fluctuations of 0.7 ± 0.1 Å, larger than for other helices, e. g., 0.5 ± 0.1 Å for helix A. Results also reflect the weak packing of helix C against the rest of the protein through only 65% of the number of close contacts formed by the best packed α-helix, the C-terminal helix D.

^{15}N order parameters

Global structural rearrangements may preclude the characterization of intrinsic backbone dynamics from the calculated fluctuations. Another descriptor of the motional freedom of the protein backbone was, therefore defined from the relaxation of bond rotation. The autocorrelation function for relaxation and the corresponding order parameters were determined from expressions 11 and 12, introduced in the Methods section. The trajectory intervals for calculation were selected, as described above, according to criteria for structural stability.

Time autocorrelation functions and order parameters were calculated only for apo N-sTnC, whose backbone dynamics has been characterized experimentally using NMR techniques (Gagne 1998). Similar to previous studies of proteins (Chandrasekhar et al., 1992; Eriksson et al., 1995;

Wriggers et al., 1998), most residues were found to undergo fast librations, efficiently sampled in the simulation. The corresponding autocorrelation functions have a sharp initial decay, followed by a plateau that extends over the entire correlation time. Convergence was not attained for Ser-2 and Gln-51, which are located in flexible regions, at the N-terminus and in the linker, respectively. The autocorrelation functions for these residues have a continuous decay throughout the correlation time interval.

Most residues located in α-helical regions and in Ca^{2+}-bound loops have order parameters larger than 0.84 (Fig. 14). The highest rotational freedom, corresponding to order parameters as low as 0.56, was found for Ca^{2+}-free loops, and for linker and terminal residues.

The difference between the calculated and the NMR order parameters is 0.03 ± 0.07 units, and indicates a good quantitative agreement. More than 90% of the computed order parameters are within two standard deviations from the experimental values. Exceptions include residues located in flexible parts of the protein, i.e., Met-3, Thr-4, Gly-71, and Lys-87, which have higher calculated order parameters. Although this difference may be due to insufficient sampling of specific slow motions in the simulation, the reasons for such deviations from the experiment are not yet clear.

Helpful and stimulating discussions with Professor Harel Weinstein are gratefully acknowledged.

REFERENCES

Amadei, A., A. B. Linssen, and H. J. Berendsen. 1993. Essential dynamics of proteins. *Proteins*. 17:412–425.

Bahar, I., A. R. Atilgan, M. C. Demirel, and B. Erman. 1998. Vibrational dynamics of folded proteins: significance of slow and fast motions in relationship to function. *Phys. Rev. Lett*. 80:2733–2736.

Balsera, M. A., W. Wriggers, Y. Oono, and K. Schulten. 1996. Principal component analysis and long time protein dynamics. *J. Phys. Chem*. 100:2567–2572.

Biosym Technologies 1998. InsightII, version 97.2.

Brooks, B., R. E. Bruccoleri, B. D. Olafson, D. J. States, S. Swaminathan, and M. Karplus. 1983. CHARMM: A program for macromolecular energy, minimization, and dynamics calculations. *J. Comp. Chem*. 4:187–217.

Brooks, B. R., and M. Karplus. 1985. Normal modes for specific motions of macromolecules: Application to the hinge-bending mode of lysozyme. *Proc. Natl. Acad. Sci. USA*. 82:4995–4999.

Brooks, C. L. I., M. Karplus, and B. M. Pettitt. 1988. A theoretical perspective of dynamics, structure, and thermodynamics. John Wiley & Sons Inc., New York.

Brooks, B. R., D. Janezic, and M. Karplus. 1995. Harmonic analysis of large systems. I Methodology. *J. Comp. Chem*. 16:1522–1542.

Chandrasekhar, I., G. M. Clore, A. Szabo, A. M. Gronenborn, and B. R. Brooks. 1992. A 500 ps molecular dynamics simulation study of interleukin-1β in water. *J. Mol. Biol*. 226:239–250.

Clarage, J. B., T. D. Romo, B. K. Andrews, B. M. Pettitt, and J. N. Phillips, Jr. 1995. A sampling problem in molecular dynamics simulations of macromolecules. *Proc. Natl. Acad. Sci. USA*. 92:3288–3292.

Cohen, C. 1975. The protein switch of muscle contraction. *Sci. Am*. 233:36–45.

Eriksson, M. A. L., T. Hard, and L. Nilsson. 1995. Molecular dynamics simulations of the glucocorticoid receptor DNA-binding domain in complex with DNA and free in solution. *Biophys. J*. 68:402–426.

Evenas, J., S. Forsen, A. Malmendal, and M. Akke. 1999. Backbone dynamics and energetics of a calmodulin domain mutant exchanging between closed and open conformations. *J. Mol. Biol*. 289:603–617.

Fersht, A. 1985. Enzyme structure and mechanism. W. H. Freeman and Company, New York.

Gagne, S. M., S. Tsuda, M. X. Li, L. B. Smillie, and B. D. Sykes. 1995. Structures of the troponin C regulatory domains in the apo and calcium-saturated states. *Nat. Struct. Biol*. 2:784–789.

Gagne, S. M., M. X. Li, and B. D. Sykes. 1997. Mechanism of direct coupling between binding and induced structural change in regulatory calcium binding proteins. *Biochemistry*. 36:4386–4392.

Gagne, S. M., S. Tsuda, L. Spyracopoulos, L. E. Kay, and B. D. Sykes. 1998. Backbone and methyl dynamics of the regulatory domain of troponin C: anisotropic rotational diffusion and contribution of conformational entropy to calcium affinity. *J. Mol. Biol*. 278:667–686.

Gellman, S. H. 1991. On the role of methionine residues in the sequence-independent recognition of nonpolar protein surfaces. *Biochemistry*. 30:6633–6636.

Grabareck, Z., W. Drabikowski, P. C. Leavis, S. S. Rosenfeld, and J. Gergely. 1981. Proteolytic fragments of troponin C. *J. Biol. Chem*. 256:13121–13127.

Grabarek, Z., R. Y. Tan, J. Wang, T. Tao, and J. Gergely. 1990. Inhibition of mutant troponin C activity by an intradomian disulfide bond. *Nature*. 345:132–135.

Hayward, S., A. Kitao, and H. J. Berendsen. 1997. Model-free methods of analyzing domain motions in proteins from simulation: a comparison of normal mode analysis and molecular dynamics simulation of lysozyme. *Proteins*. 27:425–437.

Herzberg, O., and M. N. G. James. 1988. Refined crystal structure of troponin C from turkey skeletal muscle at 2.0 Å resolution. *J. Mol. Biol*. 203:761–779.

Houdusse, A., M. L. Love, R. Dominguez, Z. Grabareck, and C. Cohen. 1997. Structures of four Ca^{2+}-bound troponin C at 2.0 Å resolution: further insights into the Ca^{2+}-switch in the calmodulin superfamily. *Structure*. 5:1695–1711.

Janezic, D., and B. R. Brooks. 1995a. Harmonic analysis of large systems. II Comparison of different protein models. *J. Comp. Chem*. 16:1543–1553.

Janezic, D., R. M. Venable, and B. R. Brooks. 1995b. Harmonic analysis of large systems. III Comparison with molecular dynamics. *J. Comp. Chem*. 16:1554–1566.

Jorgensen, W. L., J. Chadrasekhar, J. D. Madura, R. W. Impey, and M. L. Klein. 1983. Comparison of simple potential functions for simualting liquid water. *J. Chem. Phys*. 79:926–935.

Kabsch, W. 1976. A solution for the best rotation to relate two sets of vectors. *Acta Crystallogr. A*. 32:922–923.

Kretsinger, R. H. 1980. Structure and evolution of calcium-modulated proteins. *CRC Crit. Rev. Biochem*. 8:119–174.

Leavis, P. C., and J. Gergely. 1984. Thin filament proteins and thin filament-linked regulation of vertebrate muscle contraction. *CRC Crit. Rev. Biochem*. 16:235–305.

Li, M. X., S. M. Gagne, S. Tsuda, C. M. Kay, L. B. Smillie, and B. D. Sykes. 1995. Calcium binding to the regulatory N-domain of skeletal muscle troponin C occurs in a stepwise manner. *Biochemistry*. 34:8330–8340.

Li, M. X., S. M. Gagne, L. Spyracopoulos, C. P. A. Kloks, G. Audette, M. Chandra, R. J. Solaro, L. B. Smillie, and B. D. Sykes. 1997. NMR studies of Ca^{2+} binding to the regulatory domains of cardiac and E41A skeletal muscle troponin C reveal the importance of site I to energetics of the induced structural changes. *Biochemistry*. 36:12519–12525.

Liebman, M. N., C. A. Venanzi, and H. Weinstein. 1985. Structural analysis of carboxypeptidase A and its complexes with inhibitors as a basis for modeling enzyme recognition and specificity. *Biopolymers*. 24:1721–1758.

Lipari, G., and A. Szabo. 1982. Model-free approach to the interpretation of nuclear magnetic-resonance relaxation in macromolecules. *J. Am. Chem. Soc*. 104:4546–4559.

MacKerell, A. D., Jr., D. Bashford, M. Bellott, R. L. Dunbrack, J. D. Evanseck, M. J. Field, S. Fischer, J. Gao, H. Guo, S. Ha, D. Joseph-McCarthy, L. Kuchnir, K. Kuczera, F. T. K. Lau, C. Mattos, S. Michnick, T. Ngo, D. T. Nguyen, D. Prodhom, W. E. Reicher III, B. Roux, M. Schlenkrick, J. C. Smith, R. State, J. Straub, M. Watanabe, J. Wiorkiewicz-Kuczera, D. Yin, and M. Karplus. 1998. All-atom empirical potential for molecular modeling and dynamics studies of proteins. *J. Phys. Chem. B*. 102:3586–3616.

McCammon, J. A., and S. C. Harvey. 1991. Dynamics of proteins and nucleic acids. Cambridge University Press., Cambridge.

McKay, R. T., B. P. Tripet, R. S. Hodges, and B. D. Sykes. 1997. Interaction of the second binding region of troponin I with the regulatory domain of skeletal muscle troponin C as determined by NMR spectroscopy. *J. Biol. Chem.* 272:28494–28500.

McKay, R. T., J. R. Pearlstone, D. C. Corson, S. M. Gagne, L. B. Smillie, and B. D. Sykes. 1998. Structure and interaction site of the regulatory domain of troponin-C when complexed with the 96–148 region of troponin-I. *Biochemistry*. 37:12419–12430.

Meador, W. E., A. R. Means, and F. A. Quiocho. 1993. Modulation of calmodulin plasticity in molecular recognition on the basis of x-ray structures. *Science*. 262:1718–1721.

Meyer, D. F., Y. Mabuchi, and Z. Grabarek. 1996. The role of Phe-92 in the Ca^{2+}-induced conformational transition in the C-terminal domain of calmodulin. *J. Biol. Chem.* 271:11284–11290.

Mezei, M. 1997. Optimal position of the solute for simulations. *J. Comp. Chem.* 18:812–815.

Ohya, Y., and D. Botstein. 1994. Diverse essential functions revealed by complementing yeast calmodulin mutants. *Science*. 263:963–966.

Nelson, M. R., and W. J. Chazin. 1998. An interaction-based analysis of Ca^{2+}-sensor proteins. *Protein Sci.* 7:270–282.

Peersen, O. B., T. S. Madsen, and J. J. Falke. 1997. Intermolecular tuning of calmodulin by target peptides and proteins: differential effects on Ca^{2+} binding and implications for kinase activation. *Protein Sci.* 6:794–807.

Pitici, F. 1999. Structural and dynamic determinants for calcium-dependent properties of troponin-C and calmodulin: a computational study. Ph.D. thesis. Mount Sinai School of Medicine of NYU, New York. 105 pp.

Pitici, F. 2001. Ca^{2+}-sensing mechanisms in calmodulin and troponin-C.*Biophys. J.* 80:397a (Abstr.).

Porumb, T., P. Yau, T. S. Harvey, and M. Ikura. 1994. A calmodulin-target peptide hybrid molecule with unique calcium-binding properties. *Protein Eng.* 7:109–115.

Ruegg, J. C. 1986. Calcium in Muscle Activation: A Comparative Approach, 2nd ed. W. Burggren, S. Ishii, K. Johansen, H. Langer, G. Neuweuler, D. J. Randall, editors. Springer-Verlag, Berlin. 44–48.

Ryckaert, J. P., G. Ciccotti, and H. J. C. Berendsen. 1977. Numerical integration of the Cartesian equations of motion of a system with constraints: molecular dynamics of n-alkanes. *J. Comp. Phys.* 23:327–341.

Sali, A., R. Sanchez, and A. Badretdinov. 1997. MODELLER - a program for protein structure modeling, version 4.

Slupsky, C. M., and B. D. Sykes. 1995. NMR solution structure of calcium-saturated skeletal muscle troponin C. *Biochemistry*. 34:15953–15964.

Strynadka, N. C. J., M. Chernaia, A. R. Sielecki, M. Li, L. B. Smillie, and M. N. G. James. 1997. Structural details of a calcium induced molecular switch: x-ray crystallographic analysis of the calcium-saturated N-terminal domain of troponin C at 1.7 Å resolution. *J. Mol. Biol.* 273:238–255.

Thomas, K. A., G. M. Smith, T. B. Thomas, and R. J. Feldmann. 1982. Electronic distributions within protein phenylalanine aromatic rings are reflected by the three-dimensional oxygen atom environments. *Proc. Natl. Acad. Sci. USA*. 79:4843–4847.

Tirion, M. M., and D. ben-Avraham. 1993. Normal mode analysis of G-actin. *J. Mol. Biol.* 230:186–195.

van Aalten, D. M. F., A. Amadei, A. B. M. Linssen, V. G. H. Eijsink, G. Vriend, and H. J. C. Berendsen. 1995a. The essential dynamics of thermolysin: confirmation of the hinge-bending motion and comparison of simulations in vacuum and water. *Proteins*. 22:45–54.

van Aalten, D. M. F., J. B. C. Findlay, A. Amadei, and H. J. C. Berendsen. 1995b. Essential dynamics of the cellular retinol-binding protein - evidence for ligand-induced conformational changes. *Protein Eng.* 8:1129–1135.

Vogel, H., and M. Zhang. 1995. Protein engineering and NMR studies of calmodulin. *Mol. Cell. Biochem.* 149:3–15.

Vukasinovic, V. S., L. Cullen, and S. Dauner. 1997. Rational design of a calcium sensing system based on induced conformational changes of calmodulin. *J. Am. Chem. Soc.* 119:11102–11103.

Wimley, W. C., T. P. Creamer, and S. H. White. 1996. Solvation energies of amino acid side chains and backbone in a family of host-guest pentapeptides. *Biochemistry*. 35:5109–5124 .

Willis, B. T. M., and A. W. Pryor. 1975. Thermal vibrations in crystallography.Cambridge University Press, Cambridge.

Wriggers, W., E. L. Mehler, F. Pitici, H. Weinstein, and K. Schulten. 1998. Structure and dynamics of calmodulin in solution. *Biophys. J.* 74:1622–1639.

Yu, A., L. Ballard, L. Smillie, J. Pearlstone, D. Foguel, J. Silva, A. Jonas, and J. Jonas. 1999. Effects of high pressure and temperature on the wild-type and F29W mutant forms of the N-domain of avian troponin-C. *Biochim. Biophys. Acta*. 1431:53–63.

Zhang, M., M. Li, J. H. Wang, and H. J. Vogel. 1994. The effect of Met→Leu mutations on calmodulin's ability to activate cyclic nucletide phosphodiesterase. *J. Biol. Chem.* 269:15546–15552.

Zot, H. G., and J. D. Potter. 1982. A structural role for the Ca^{2+}-Mg^{2+} sites on troponin C in the regulation of muscle contraction. Preparation and properties of troponin C depleted myofibrils. *J. Biol. Chem.* 257:7678–7683.